12

Predictability and forecasting

Duane Waliser

12.1 INTRODUCTION

In April of 2002, a workshop was held that brought together participants with a wide range of geophysical expertise to focus on the problem of sub-seasonal predictability (Schubert *et al.*, 2002). This workshop marked a relatively important milestone in the development of our predictive capability of the atmosphere, ocean, and land systems. The fact that it lured scientists with expertise in modeling, theory, and observations, as well as operational forecasters and funding agency administrators indicated that we had reached the point where sub-seasonal variability presented itself as more than a theoretical concern or vaguely observed set of phenomena. In fact, the need for such a workshop was based on the recognition that a number of sub-seasonal features could likely provide near-term opportunities for improving long-lead forecast skill. One of the keynote speakers, H. van den Dool, brought to the participants' attention the early foresight that John von Neumann (1955) had of the expected progress to be made in the area of "long-range" forecasting. In terms of present-day terminology, von Neumann recognized (see Appendix I for excerpt) that the first gains to be made in the area of [atmospheric] prediction were likely to be made at the short range where the initial conditions are expected to play an important role (i.e., 1950s–1970s). Following progress in this area, substantial gains would next be likely made at the very long range, meaning climate prediction, where surface boundary conditions (e.g., large-scale sea surface temperature (SST)) are expected to play the most important role (i.e., 1980s–1990s). Then, only after considerable understanding was obtained in each of these two extreme regimes could progress be made at the sub-seasonal timescale (e.g., 2 weeks to 2 months) where both the initial conditions and boundary conditions are expected to be important. The occurrence of this workshop and its follow-on activities (Waliser *et al.*, 2003a) indicate that by virtue of our progress with both "weather" and "climate" prediction

problems, we had reached a point where it was feasible to consider the intermediary problem of the sub-seasonal timescale.

While the workshop mentioned above included presentations and discussion of a number of sub-seasonal phenomena, including the Pacific North America pattern, North Atlantic Oscillation, Arctic Oscillation, and blocking, it was clear that the Madden–Julian Oscillation (MJO) was one of the most underexploited in terms of the likely potential for near-term gains in the area of sub-seasonal prediction, or maybe more importantly, accounting for its effects on medium-to-extended range weather prediction. This was not only due to the characteristics of the phenomena itself (e.g., see Chapter 10) and the direct impact it has on a broad region of the tropics but because of the role it plays, via tropical diabatic heating variability, on the evolution of the extra-tropics (e.g., see Chapters 2–5). In order to fully exploit the possible benefits from MJO/sub-seasonal prediction, it is obvious from the discussion in Chapter 11 that the biggest hurdle to overcome at present is the development of forecasting models that properly represent the phenomena itself. Once this is achieved, it is bound to be an important step to making further progress in weather and climate prediction. For weather, the sub-seasonal timescale offers the hope for extending (at least occasionally) the range of useful forecasts of weather and/or weather statistics, while for the seasonal and longer term climate prediction problem proper representation of the sub-seasonal timescale is a key component of the atmospheric "noise" that is an influential factor in the climate prediction problem as well as a limitation on expected skill.

The previous chapters in this book illustrate the significant influence that the MJO has on our weather and climate. As influential as the MJO is, a fundamental question yet to be adequately addressed concerns its theoretical limit of predictability. For example, it is well known that useful skill associated with deterministic prediction of most "weather" phenomena is limited to about 6–10 days (e.g., Thompson, 1957; Lorenz, 1965; 1982; Palmer, 1993; van den Dool, 1994). Similarly, it has been found that the likely limit of predictability for the El Niño Southern Oscillation (ENSO) is on the order of 12–18 months (e.g., Cane *et al.*, 1986; Graham and Barnett, 1995; Kirtman *et al.*, 1997; Barnston *et al.*, 1999). However, it is still yet to be determined what the corresponding metric is for the MJO/intraseasonal oscillation (ISO) phenomenon. The somewhat well behaved nature of the MJO/ISO (e.g., equatorially-trapped; preference for warm SSTs, seasonality) along with its intraseasonal timescale suggests that useful predictive skill might exist out to at least 15–25 days and maybe longer. Support for this suggestion comes from statistical predictive models of the MJO/ISO, which indicate useful skill out to at least 15–20 days lead time. However, as with any statistical model, these models are sorely limited in the totality of the weather/climate system they can predict, their ability to adapt to arbitrary conditions, and their ability to take advantage of known physical constraints. Additional support for this expectation comes from a few dynamic predictability studies using the twin-experiment methodology that indicates useful predictability may extend to 25–30 days or more. However, our dynamic models still have weaknesses relative to their representations of the MJO so these values also have to be considered with caution.

This chapter will review the progress that has been made regarding our capabilities of predicting the MJO via empirical and dynamical means and our understanding of its predictability characteristics. Note that there are a number of studies that indicate an influence of the MJO on the prediction and predictability of remote (extra-tropics) and/or secondary circulations (e.g., hurricanes). These will not be discussed directly but will be alluded to, and in some cases cited, in Section 12.6. In the following section, a review of empirical methods for forecasting the MJO will be presented. In Section 12.3, an analogous discussion will be presented for forecasts based on dynamical (i.e., numerical weather prediction) models. In Section 12.4, issues regarding the inherent predictability of the MJO will be discussed. In Section 12.5, present-day efforts of real-time MJO forecasting will be described. Section 12.6 concludes with a discussion of the outstanding issues and questions regarding future progress in this area.

12.2 EMPIRICAL MODELS

By the late 1980s, many characteristics of the MJO were fairly well documented and it was clear that it was a somewhat well defined phenomenon with a number of reproducible features from one event to another as well as in events from one year to the next. Given this, and the degree that research had shown a number of important interactions of the MJO with other features of our weather and climate system, it was an obvious step to begin to consider MJO forecasting in more earnest. Since numerical weather and climate models typically had a relatively poor representation of the MJO at the time, a natural avenue to consider was the development of empirical models. Along with likely providing more skillful forecasts than numerical methods available at the time, this avenue also provided a means to establish an initial estimate of the predictability limit for the MJO – at least that which could be ascertained from the observations alone.

The first study along these lines was by von Storch and Xu (1990) who examined Principal Oscillating Patterns (POPs) of equatorial 200-mb velocity potential anomalies from a 2-year subinterval of a 5-year data set. Upon verifying against the data set as a whole (as well as against the remaining three years of data), they found that forecasts based on the first pair of POPs – which tended to emphasize the variability in austral summer (e.g., Figures 4.5 and 5.8) – produced forecasts that were better than persistence and appeared to have useful skill out to at about 15 days (Figure 12.1). While this was a somewhat encouraging result – at least relative to "weather", the limited length of data used combined with the non-stationary characteristics of the MJO over interannual timescales (e.g., Salby and Hendon, 1994; Hendon *et al.*, 1999) necessitated some caution in over-interpretation. Moreover, given the smoothly varying nature of the 200-hPa velocity potential, and the fact that it is only loosely related to near-surface meteorological variables (e.g., precipitation), also suggested caution in generalizing this result to other years, variables, and/or different techniques. In this regard, one might hope that given the roughly 50-day timescale of the MJO that it might be possible to have useful skill out to one-half of a

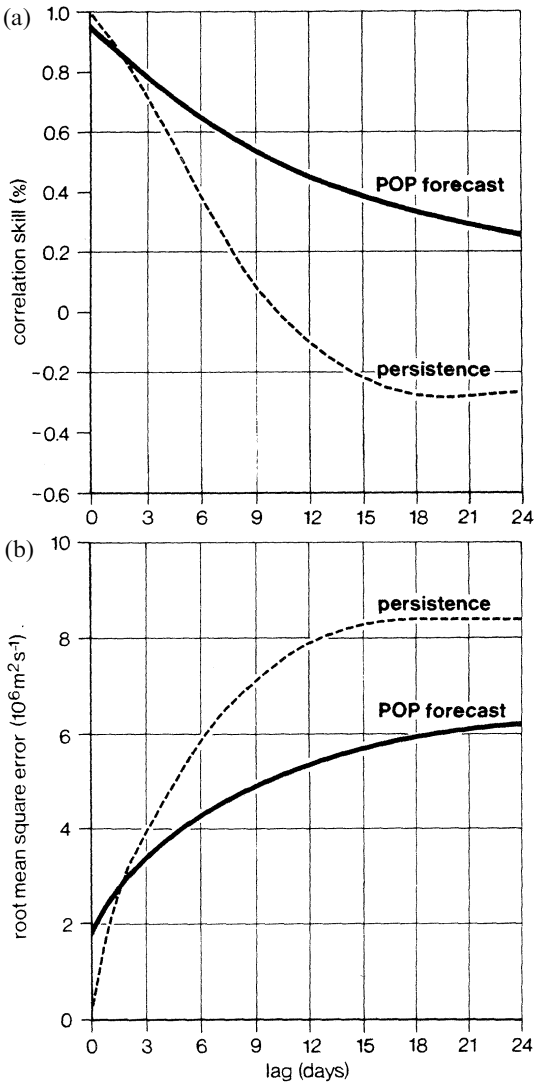

Figure 12.1. Measures of (a) correlation and (b) root-mean-square error forecast skill for persistence and the POP-based forecasting scheme developed by von Storch and Xu (1990). The skills have been derived from daily forecast experiments for the period May 1984 to April 1989. Note the model itself was developed from data between May 1986 to April 1988.

period (van den Dool and Saha, 2002) – particularly for upper level flow (e.g., 200-hPa velocity potential). Subsequent to the above, Kousky and Kayano (1993) suggested that real-time monitoring of the MJO could be achieved by projecting anomalies of a number of fields, outgoing long-wave radiation (OLR) (200-hPa velocity potential, surface pressure, etc.) onto their leading combined extended

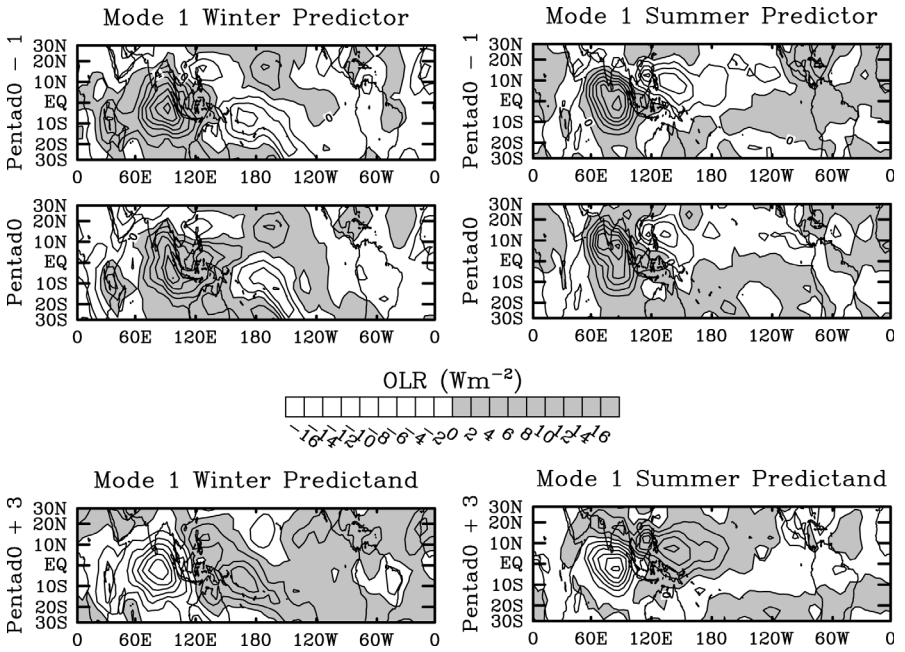

Figure 12.2. (*left column*) Mode 1 from the Singular Value Decomposition (SVD)-based MJO forecasting scheme developed by Waliser *et al*. (1999b) for the northern hemisphere winter and a 3-pented lead forecast. The top panel shows the predictor patterns for "Pentad0" (the current pentad) and "Pentad0 − 1" (the previous pentad). The bottom panel shows the associated predicted patterns for "Pentad0 + 3" (i.e., 3 pentads in the future). (*right column*) The same, except for northern hemisphere summer. Here winter (summer) is defined as November 17 to May 15 (May 16 to November 16). Note that mode 2 for each season looks similar to mode 1 but tends to be spatially in quadrature.

empirical orthogonal function patterns which would indicate the present phase and strength of the MJO in the tropical atmosphere and its likely evolution. It turns out that a number of later developments in the area of empirical MJO prediction tended to follow this suggestion in one form or another.

After a relatively long hiatus in this area, Waliser *et al*. (1999b) developed an empirical MJO forecasting method in order to use the skill results as a benchmark by which to judge the predictive skill of numerical long-range forecasts and to begin exploring the feasibility of employing such a model to augment operational long-range forecasting procedures. The model was based on a field-to-field Singular Value Decomposition that used previous and present pentads of OLR to predict future pentads of OLR (Figure 12.2). Separate models were developed for austral and boreal summer conditions (e.g., Figures 4.5 and 4.10, respectively) using 30–70-day filtered OLR data from 1979 to 1989 and validated on data from 1990 to 1996. For the validation period, the model exhibited temporal correlations to

filtered observations of about 0.5–0.9 over a significant region of the eastern hemisphere at lead times from 15 to 20 days, after which the correlation dropped rapidly with increasing lead time. Correlations against observed total anomalies were of the order of 0.3 to 0.5 over a smaller region of the eastern hemisphere. While this was an equally, if not more, encouraging result than that of von Storch and Xu (1990), discussed above, the fact that the model utilized filtered data limited its real-time applicability and in this case warranted caution in considering the result too optimistic. In concluding their study, the authors provided a number of avenues for addressing this filtering problem (i.e., being able to isolate the MJO signal from both the "weather" and the interannual climate variations). For example, it was suggested that the low-frequency variations (i.e., ENSO variability) might be removed using projections on low-order empirical orthogonal functions from coarser (e.g., monthly) data, and high-frequency signals could be removed by using longer time averages, that could even overlap to retain some aspect of the high temporal resolution (e.g., overlapping 10-day averages every 5 days). In addition, it was noted that once the low-frequency variability was removed, low-pass spatial filtering might serve as a useful mechanism for low-pass temporal filtering given that the MJO variability tends to be isolated to wave numbers 1–3 and periods of about 40–60 days.

Following the above study, there were a number of empirical MJO forecasting efforts that each produced a unique and useful approach to the problem. Lo and Hendon (2000) developed a lag regression model that uses as predictors the first two and first three principal components (PCs) of spatially filtered OLR and 200-hPa streamfunction (Ψ), respectively, to predict the evolution of the OLR and 200-hPa streamfunction anomalies associated with the austral summer MJO. In order to address the filtering problem discussed above in regards to real-time application, the data had the annual cycle, interannual and high-frequency (i.e., < 30 days) components removed separately. The annual cycle was removed by subtracting out the first three annual harmonics pointwise. The interannual (e.g., ENSO) variability was removed by developing regression equations between the OLR (and Ψ) anomalies and the PC time series from the first two EOFs of tropical SST anomalies (SSTAs). Based on these regressions and the daily SST values (interpolated from weekly data), the low-frequency components of OLR (and Ψ) that could plausibly be attributed to ENSO were removed. Subsequent to this, the high-frequency temporal components of the data were removed by subjecting the data to a T12 spectral truncation – utilizing the notion that the high-frequency temporal and high wave number spatial variations tended to occur concomitantly. The resulting intraseasonally filtered OLR and Ψ anomalies were subjected to an EOF decomposition and then time-lagged regression equations were developed for predicting, at a given lead, the PC values for the EOF modes that define the MJO (e.g., mode 1 and 2). When tested on independent data, the model exhibited useful skill (correlation ~ 0.5) for predictions of these PCs out to about 15 days (Figure 12.3), with greater skill during active vs. quiescent MJO periods. In comparisons to the filtered observed OLR data, the model exhibited correlation values around 0.3–0.4 in a fairly broad region of the equatorial Indian Ocean and maritime continent.

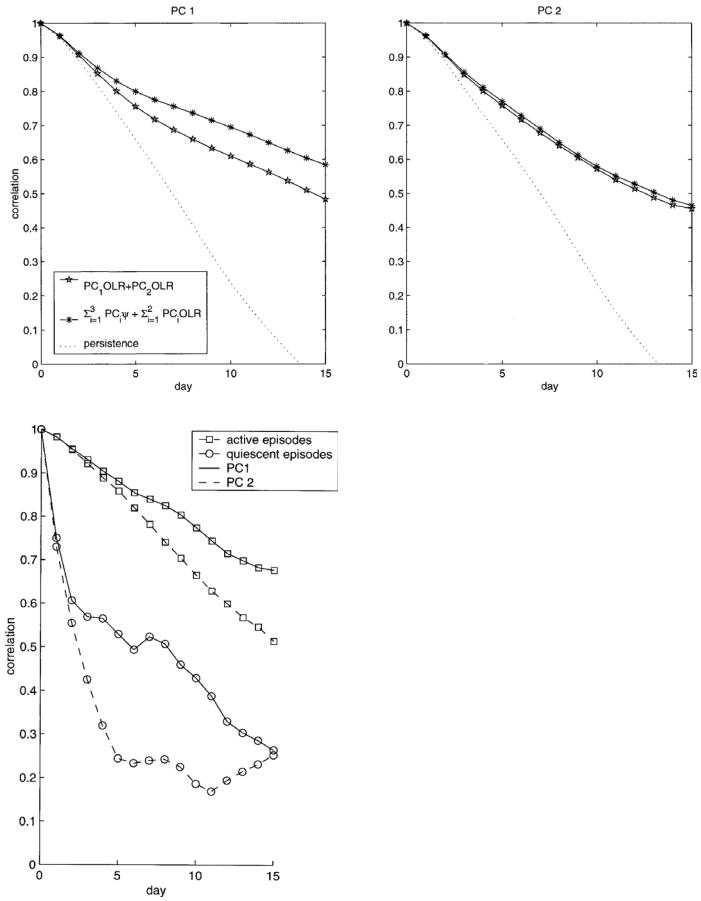

Figure 12.3. (*top*) Measure of forecast skill for the MJO forecasting scheme developed by Lo and Hendon (2000) in terms of correlations between predicted values and verifying values of the PC values associated with mode 1 (PC 1; *left*) and PC values associated with mode 2 (PC 2; *right*). Predictions were made using PC 1 and PC 2 of OLR anomalies (stars), the leading three PCs of the 200-hPa streamfunction anomalies, and leading two PCs of OLR anomalies (asterisks). Persistence is shown as the dotted curve. (*bottom*) Correlations between predicted values and verifying values of PC 1 (solid lines) and PC 2 (dashed lines) of OLR anomalies for times when the MJO was active (squares) and quiescent (circles) at the initial condition during the five winters of dependent data. Predictions were made using the leading three PCs of the 200-hPa streamfunction anomalies and leading two PCs of OLR anomalies. In all figures, correlations are shown as a function of forecast lead time and the verification is against the five winters (1984/1985–1989/1990) of independent data.

A somewhat different approach was taken by Mo (2001) who utilized empirical basis functions in time for the forecasting procedure. This was done by using a combination of singular spectrum analysis (SSA) (Vautard and Ghil, 1989) for the filtering and identification of the principal modes of variability and the maximum

entropy method (MEM) (Keppenne and Ghil, 1992) for the forecasting component. The procedure was applied to monitor and forecast outgoing longwave radiation anomalies (OLRAs) in the intraseasonal band over both the Indian–Pacific sector as well as the Pan-American region. This included variability such as the MJO, higher frequency intraseasonal modes associated with the Asian monsoon (see Chapters 2 and 3), and variability related to both of these that occurs over the US west coast (see Chapter 4). For example, in the Pacific and the Pan-American region, there were three leading modes (T-EOFs) identified with periods near 40, 22, and 18 days. In this method, the leading SSA modes (T-EOFs) are determined from a training period. The OLRA time series are then projected onto T-EOFs to obtain the principal components (T-PCs). To obtain fluctuations in a given frequency band of interest (i.e., perform filtering), a subset of the T-EOFs and the related T-PCs associated with that band are summed. This filtering procedure, based on the SSA modes, is data adaptive and there is no loss of end points. This aspect makes it particularly well suited for real-time monitoring. To perform forecasts, the MEM is used to determine the autoregressive coefficients from the training period. These coefficients are used to forecast the T-PCs at future leads. The summation of the T-EOFs and T-PCs related to three retained modes used in the filtering process gives the predicted OLRAs. When tested on 8 years of independent December–February and June–August OLRA data, the averaged correlation over the tropics between the predicted and the observed anomalies was 0.65 (range 0.48–0.78) at the lead times of four pentads (20 days). An example of the forecast skill for the equatorial region for the 1992/1993 winter is given in Figure 12.4. The main activity in this record occurs prior to February 1993 and extends between the Indian and central Pacific Oceans. Although the model amplitudes are weaker that the observations, a feature not uncommon amongst the empirical models, the spatial–temporal structure is well captured out to the pentad-4 forecast.

In a quite different approach, Wheeler and Weickmann (2001) utilized tropical wave theory (Matsuno, 1966) as the basis for their filtering and forecasting technique. Essentially, a space–time Fourier analysis is performed on daily OLR data for a given time–longitude section of interest in the tropics. In a previous study, Wheeler and Kiladis (1999) showed that the spectrum from such an analysis exhibits variability that is associated with the modes that one would expect from theoretical considerations (e.g., Kelvin waves and mixed Rossby–gravity waves), as well as the expected peak of variability around wave numbers 1–3 and 40–60 days associated with the MJO. In order to monitor and predict the evolution of a given mode of interest, the specific zonal wave numbers and frequencies associated with the mode(s) of interest are retained and then the modified spectrum is inverse-Fourier analyzed. Figure 12.5 shows how the filtered values obtained for times before the end of the data set can be used for monitoring the activity of a given mode, while the filtered fields obtained for times after the end point may be used as a forecast. This idea is akin to an ocean tidal forecast, which in that case is based on harmonic analysis in time only and of course much sharper frequencies of variability. For prediction, the method exhibits useful skill for the MJO out to about 15–20 days. An advantage is that the method readily provides

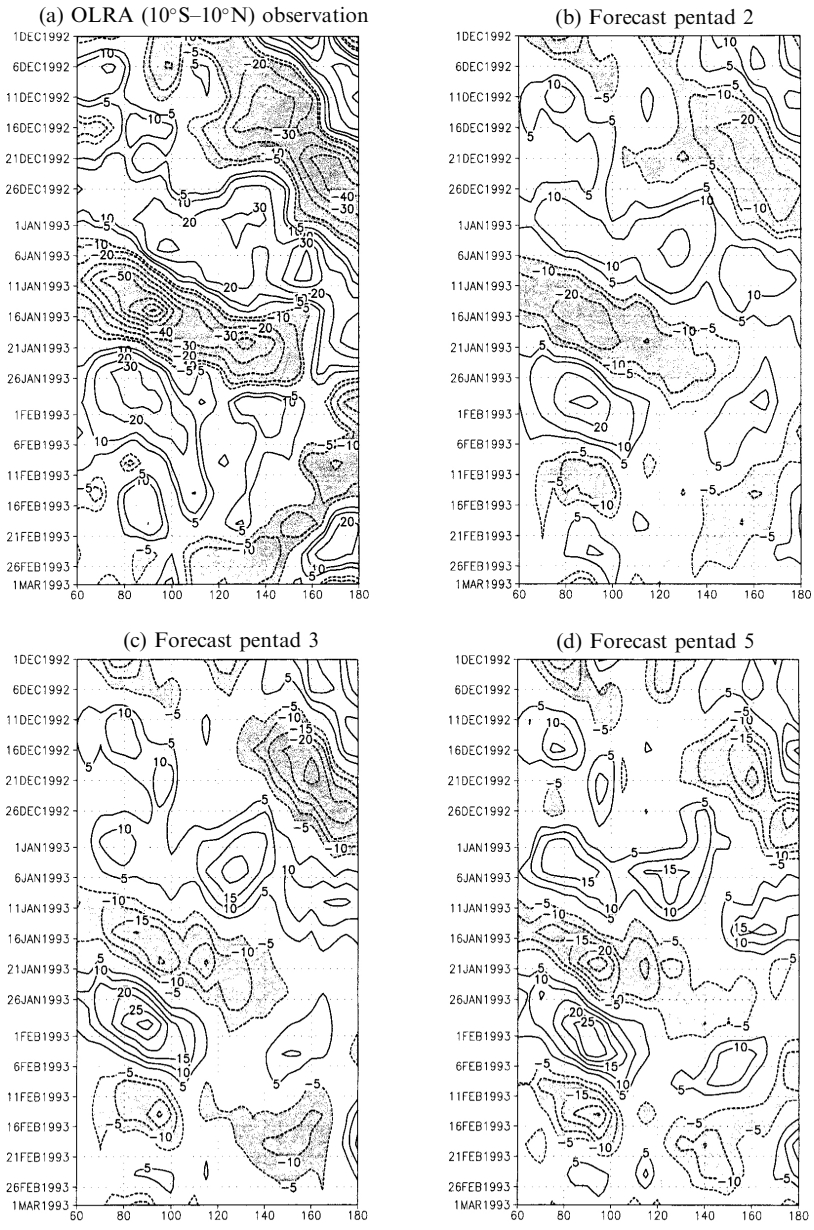

Figure 12.4. (a) 10–90-day filtered OLRAs averaged from 10°S to 10°N based on the minimum bias window for the 1992/1993 winter from observations. Contour interval is $10\,W\,m^{-2}$. Contours 25 and $5\,W\,m^{-2}$ are added. Negative values are shaded and zero contours are omitted. (b) Same as (a), but for 10-day (pendad 2) forecasts based on the empirical model developed by Mo (2001) verified on that day. (c) Same as (b), but for 15-day forecasts (pentad 3). Contour interval is $5\,W\,m^{-3}$. (d) Same as (c), but for 20-day (pentad 4) forecasts.

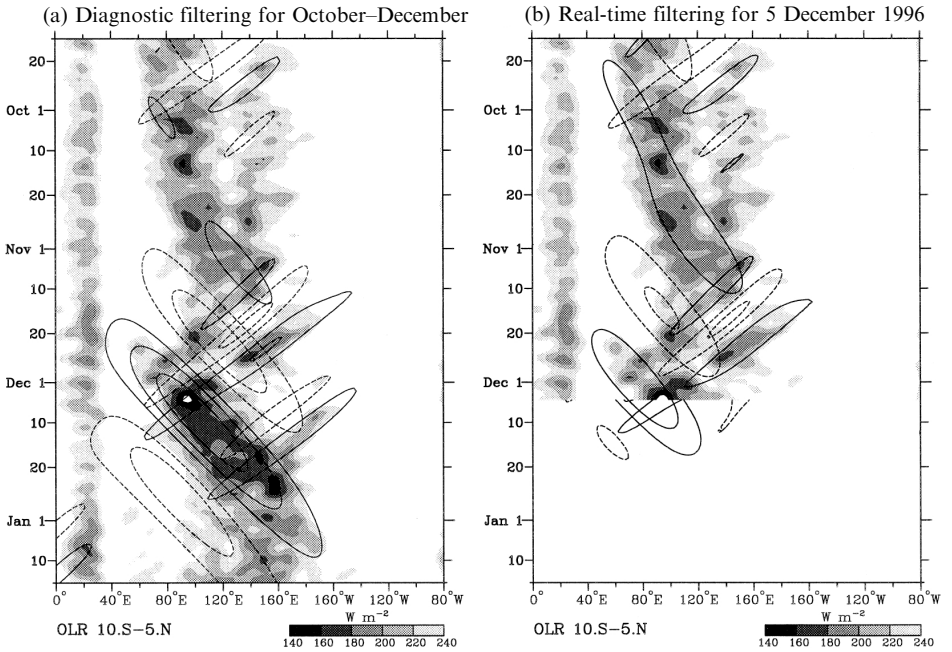

Figure 12.5. (a) Time–longitude plot of the total OLR (with R21 spatial truncation, and a 1–2–1 filter applied in time) and filtered OLRAs averaged between 10°S and 5°N during late 1996 to early 1997. Shading is for the total OLR, and contours are for the diagnostically filtered anomalies of the MJO and $n = 1$ equatorial Rossby (ER) wave. Solid contours represent negative OLRAs, while dashed contours are for positive anomalies, with the contour interval for both wave filtered bands being $10\,\mathrm{W\,m^{-2}}$, and the zero contour omitted. (b) Same as in (a) except that the filtering was performed with the last day of data being that from 5 December 1996. After 5 December, when the real-time filtered anomalies are continued into the future as a forecast, the contour interval is halved.
From Wheeler and Weickman (2001).

predictions of other well-defined, typically higher frequency, modes of large-scale tropical variability.

In an effort that focused on active and break conditions of the Indian summer monsoon, Goswami and Xavier (2003), noted that all active (break) conditions go over to break (active) phases after about 15–20 days (see Figure 2.3). The events would be highly predictable if the transitions from active to break (or vice versa) were all identical. However, the rate of transition, the magnitude of the next minimum (or maximum), and the timing of achieving the minimum (maximum) of the next phase vary from event to event. Using the rainfall-based index illustrated in Figure 2.3 and their definition of active and break conditions (see Chapter 2), Goswami and Xavier calculated the typical (i.e., ensemble average) transition from active to break (and break to active) conditions as a function of lead time. The typical size of these transitions – referred to as the "signal", and their associated intra-ensemble variance – referred to as the (ensemble) "spread", are shown in

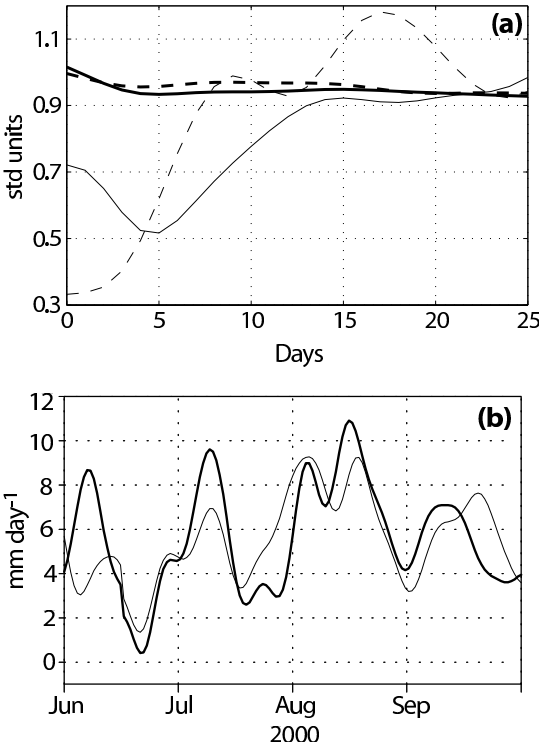

Figure 12.6. (a) The thick dashed (solid) line is the monsoon ISO "signal" starting from troughs (peaks) of the index (see Figure 2.3). The thin dashed (solid) line is the variance (or spread) of ensemble members as a function of days from the initial date corresponding to all troughs (peaks) of the index representing transitions from break to active (active to break). (b) Time series of 18-day predictions (thin line) and observations (thick line) of the rainfall (mm day^{-1}) averaged over the monsoon trough region for June–September 2000.
From Goswami and Xavier (2003).

Figure 12.6(a). While the variability among break to active transitions become as large as the associated signal in less than 10 days, it takes more than 20 days for the variance among active to break transitions to become as large as the signal. Circulation parameters such as the 850-hPa relative vorticity over the monsoon trough region also lead to the same conclusion (not shown). These results indicate that monsoon breaks are intrinsically more predictable than active monsoon conditions. Similar results were found by Waliser *et al.* (2003c) using an ensemble of twin-predictability GCM experiments (see Section 12.4). To explore the practical consequences of these results, Goswami and Xavier constructed an empirical multiple regression model for the first four PCs of 10–90-day filtered CMAP using the first four PCs of filtered rainfall data and the first two PCs of filtered surface pressure as predictors, and showed that useful prediction of monsoon breaks, up to 18 days in advance, could be made while useful forecast of active conditions could be

made with lead times of only about 10 days. Eighteen-day forecasts of filtered precipitation averaged over central India and the northern Bay of Bengal (70°E–85°E, 10°N–22°N) for June to September 2000 are shown in the lower panel of Figure 12.6.

The above discussion gives a flavor of the types of empirical MJO modeling that have been developed to date and their associated levels of forecast skill. However, there is a number of additional empirical modeling studies worth describing that are presently associated with real-time efforts and these are discussed in Section 12.5. In regard to the studies above, it is useful to emphasize at this point that the skill associated with the techniques above in almost all cases has yet to be demonstrated by numerical forecast techniques (e.g., Waliser *et al.*, 1999b; Jones *et al.*, 2000; Lo and Hendon, 2000; Wheeler and Weickmann, 2001). Moreover, it is worth highlighting that in no cases are these schemes physical in nature or based on very complex techniques, and they are all based on linear methods. Thus, it is likely that we may not have yet developed and demonstrated models that have saturated the skill potential for empirical forecasting methods. In addition, it is also worth highlighting that MJO events are at best quasi-periodic in nature, meaning here that the atmosphere can be relatively quiescent in regards to MJO variability with an event suddenly developing. Each of the models above would tend to perform relatively poorly at forecasting this initial development, as they all tend to rely on the periodic nature of the MJO to forecast its evolution. For these scenarios, as well as for dealing with the heterogeneity of MJO events, it will be vital to improve our dynamic models, as they are likely to be the best means to deal with these sorts of issues. In any case, the above sorts of studies provide a useful benchmark in forecast skill for our dynamical models and suggest, based on the observations alone, that the MJO should be predictable with lead times of at least 2–3 weeks.

12.3 DYNAMICAL FORECAST MODELS

To date, there have only been a handful of studies that have examined forecast skill (i.e., verified against observations) from dynamical models. This has probably stemmed from what amounted to: (a) considerably less overall interest in forecasting the intraseasonal timescale relative to weather and ENSO, (b) the difficulty and resources required to produce an adequate sample of very long-range weather forecasts (at least 30 days), (c) the pessimism and known challenges associated with tropical weather forecasting in general, and (d) the indications that neither our forecast nor climate simulation models were very adept at simulating the MJO (see Chapter 11). In any case, as part of a more generalized forecast skill study of the planetary-scale divergent circulation, Chen and Alpert (1990) examined the MJO forecast skill from one year (June 1987–May 1988) of daily 10-day forecasts from the US National Meteorological Center's [NMC; now National Center for Environmental Prediction (NCEP)] medium-range forecast (MRF) model (based partly on MRF86 and MRF87) in terms of the 200-hPa velocity potential. In their analysis, the MRF's forecast skill, measured in terms of spatial correlations of 200-hPa

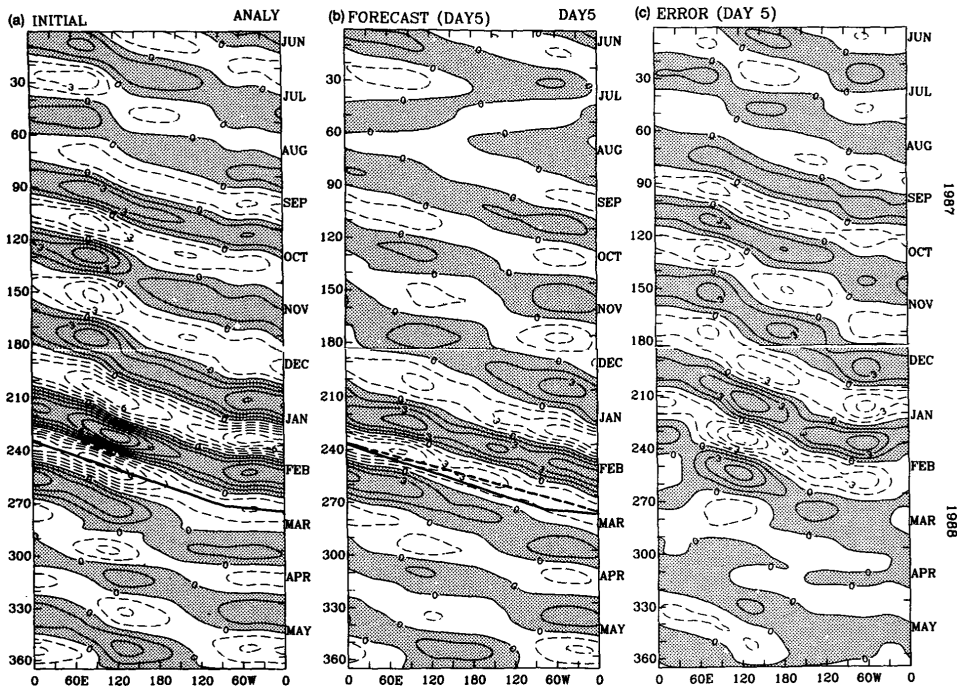

Figure 12.7. Equatorial time–longitude diagram of 200-hPa velocity potential anomalies constructed from the first two EOF modes of the data. In this case, the EOF was done separately for each lead time. Values are shown for: (a) initial conditions, (b) day 5 forecasts, and (c) day 5 forecast errors. The solid line connects maximum initial condition 200-hPa velocity potential anomalies for one-half of a life cycle of the ISO during winter in (a). The dashed line connects maximum 200-hPa velocity potential anomalies of the day 5 forecast in (b). The solid line of (a) is also shown in (b) for comparison. The contour interval is $1.0 \times 10^6\ \mathrm{m^2\ s^{-1}}$.
From Chen and Alpert (1990).

velocity potential between 50°N–50°S, declined to about 0.6 by forecast day 6 and 0.4 by forecast day 9. This relatively poor skill was attributed to: (1) the inability of the model to maintain MJO variability during a forecast (thus the model probably did not intrinsically exhibit or support an MJO of its own) and (2) the model's tendency to propagate MJO anomalies too fast. This latter aspect is illustrated in Figure 12.7. The left panel illustrates the observed 200-hPa velocity potential with a line overlaid to indicate the observed phase speed of one of the stronger events. The middle panel illustrates the model forecast values at a lead time of 5 days with the same line overlaid from the left panel which shows quite clearly that the model is propagating the anomalies too fast. Lau and Chang (1992) analyzed one season (14 December 1986–31 March 1987) of 30-day global forecasts derived from a set of Dynamical Extended Range Forecasts (DERFs) from a research version of the MRF86 model mentioned above. Their results, depicted in Figure 12.8, showed

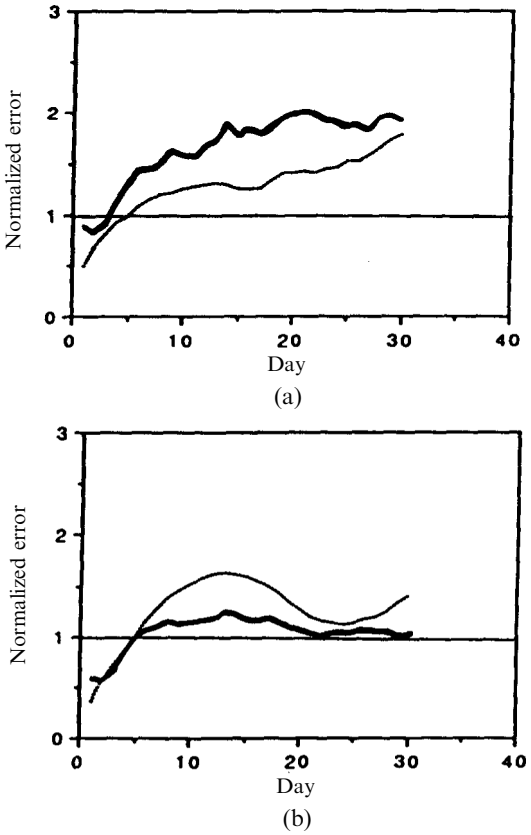

Figure 12.8. Forecast (thick) and persistence (thin) error curves for the first EOF of the global velocity potential (referred to as the tropical mode) from the NMC (now NCEP) Phase II DERF experiment. This data set consisted of 108 30-day forecasts for the period 14 December 1986–31 March 1987. The top (bottom) shows the errors for a period of weak (strong) MJO activity. The horizontal lines indicate the level of natural variability for the corresponding periods.
From Lau and Chang (1992).

that the forecast model had significant skill in predicting the global pattern of ISV in 200-hPa velocity potential and streamfunction for up to 10 days lead time, with the error growth of tropical and extra-tropical low-frequency modes less than persistence when the amplitude of the MJO was large and vice versa when the amplitude was small.

Both Hendon *et al.* (2000) and Jones *et al.* (2000) analyzed a more recent DERF experiment which used the reanalysis version (Kalnay *et al.*, 1996) of the NCEP MRF model (Schemm *et al.*, 1996). This experiment included 50-day forecasts made once a day for the period January 1985–February 1990. In both studies, the focus was on the northern hemisphere winter season. Using different analysis and

filtering techniques for identifying the MJO within the forecasts, and thus for assessing forecast skill against observations, both studies concluded that this version of the NCEP MRF model also exhibited a rather poor MJO forecast skill. Specifically, the upper panel of Figure 12.9 from Jones *et al.* (2000) shows that the anomaly correlations of intraseasonally filtered values of 200-hPa zonal wind, zonally-averaged along the equator, declined from about 0.6 on day 3 to 0.2 by day 10. The lower panel shows that the model exhibited a forecast skill that was slightly better (worse) when the MJO was particularly active (weak; i.e., null case) and that the model skill might have some dependence on the phase of the MJO (see caption for details). The rather poor forecast skill was attributed to the development of systematic errors in the forecast upper-level winds, particularly over the eastern Pacific and, as above, due to the inability of this model to maintain/simulate a robust MJO phenomena itself. For example, a diagnosis of the model's representation of the MJO from a 10-year simulation using the same model showed an MJO-like phenomenon but one that was significantly less intense and propagated considerably faster than the observed phenomenon (Jones *et al.*, 2000).

The rather detailed analysis by Hendon *et al.* (2000) showed that the forecasts initialized during very active episodes of the MJO did not reproduce the observed eastward propagation of the tropical convection and circulation anomalies, rather the anomalies would typically weaken in place and even retrograde in some cases. Typically it was found that the convective anomalies would decay almost completely by day 7 of the forecast, and in nearly the same time systematic errors in the extra-tropical 200-hPa streamfunction became fully developed. They argued that the errors in the latter developed due to the collapse of the tropical heating anomalies and thus the development of an error in the Rossby wave source emanating from the tropics. Due to the types of errors, which are greatest for the largest MJO anomalies, and likely due to their categorization of active events, their analysis showed that forecast skill in the tropics and northern hemisphere extra-tropics was actually worse during the active MJO events vs. periods that exhibited very little MJO activity (Figure 12.10 – see caption for details). The above studies point to the need for the forecast models to not only have a proper representation of MJO anomalies but also to produce an unbiased mean state so initialization errors and their subsequent evolution/adjustment do not contaminate the forecast over these relatively long lead times.

In a totally independent line of research, T. N. Krishnamurti produced a number of studies in the early 1990s that examined MJO forecast skill as it relates to active and break periods of the Asian summer monsoon. Underlying these studies is the development and application of a unique and potentially promising avenue for forecasting "low-frequency modes" (as they are referred to in these studies). In the first study, Krishnamurti *et al.* (1990) laid the groundwork for the method which argues that part of the loss of forecast skill associated with low-frequency modes such as the MJO during a forecast comes about from the errors and evolution of high wave number/frequency variability. If the forecast objective is primarily the prediction of low-frequency variability (e.g., active and break periods of the monsoon), then it is plausible to filter the initial state in order to remove all but

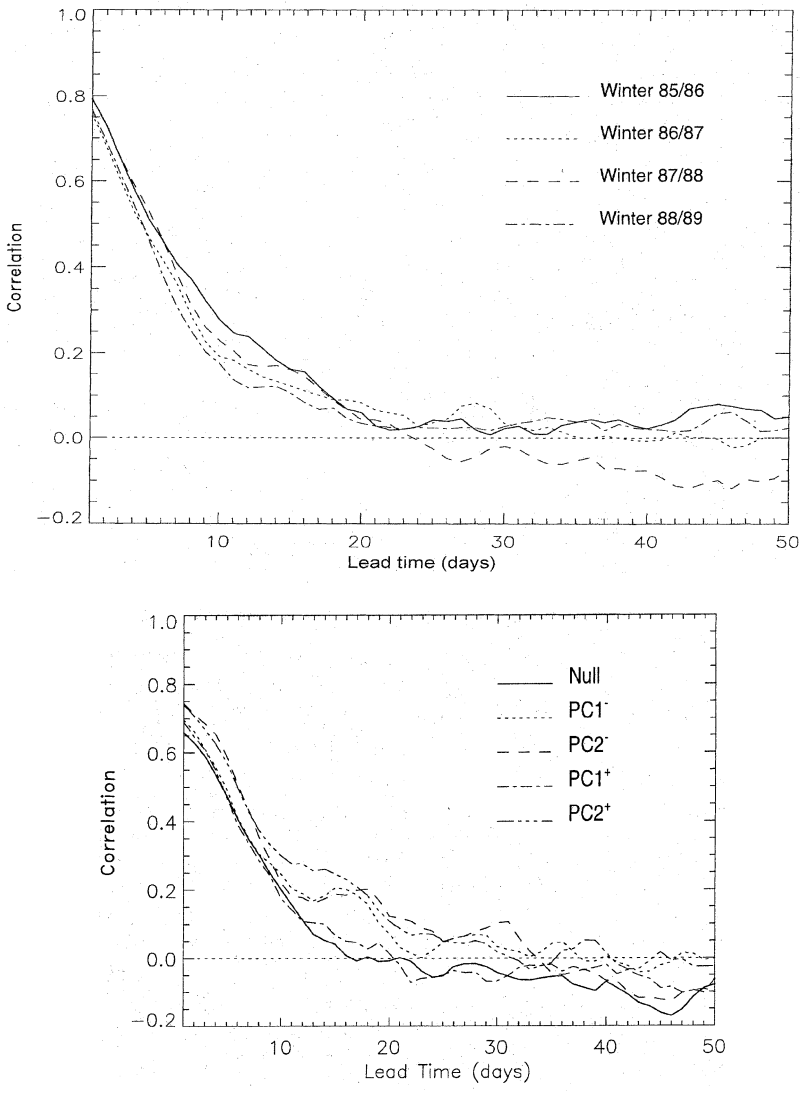

Figure 12.9. Zonal average along the equator of the anomaly correlation between the forecast and verification of 200-hPa zonal velocity as a function of lead time. Forecast data are based on the DERF experiment (Schemm *et al.*, 1996) which used the reanalysis version (Kalnay *et al.*, 1996) of the NCEP MRF model. This experiment included 50-day forecasts made once a day for the period January 1985–February 1990. Correlations are shown for (*top*) each winter season separately and for (*bottom*) the forecast separated into four different phases of the MJO, and quiescent (i.e., null) cases, using the PC values of the first two EOFs of intraseasonally filtered OLR. Values associated with PC 1+, PC 1−, PC 2+, and PC 2− are associated with the convective phase being located at 90°E, 120°E, 150°E, and 170°W, respectively, at the start of the forecast.
From Jones *et al.* (2000).

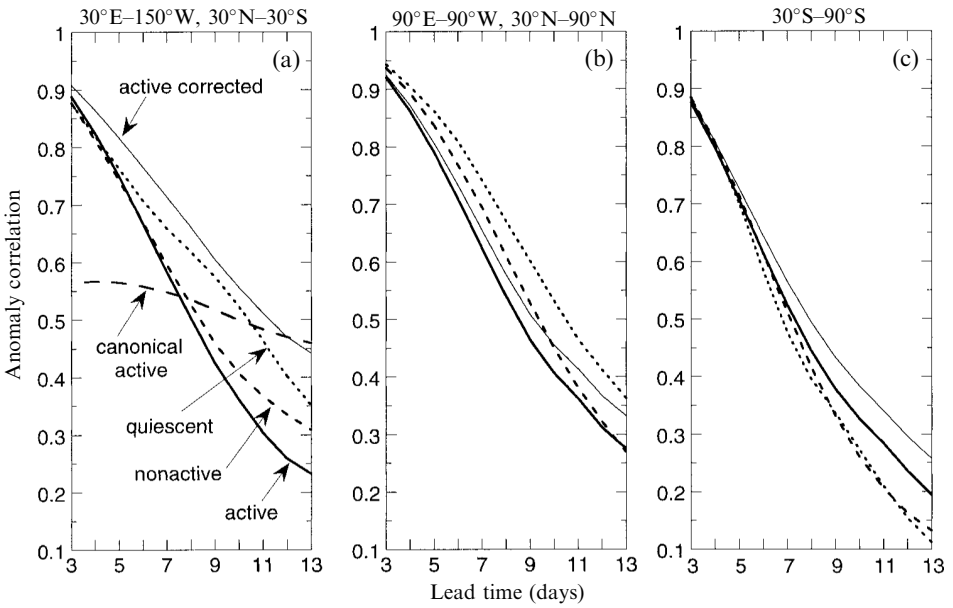

Figure 12.10. Anomaly correlations between forecasts, as functions of lead time, and verification of the 200-hPa streamfunction for: (a) the tropical region 30°N–30°S, 30°E–150°W; (b) the northern hemisphere extra-tropical region 30°–90°N, 90°E–90°W; and (c) the southern hemisphere extra-tropics 30°S–90°S. Forecast data are based on the DERF experiment (Schemm *et al.*, 1996) which used the reanalysis version (Kalnay *et al.*, 1996) of the NCEP MRF model. This experiment included 50-day forecasts made once a day for the period January 1985–February 1990. Correlations are shown for all forecasts initialized when the MJO was active and quiescent and for times when the MJO was inactive (i.e., neither active nor quiescent). Active and quiescent MJO periods were selected using the PC values of the first two EOFs of intraseasonally filtered OLR. Empirically corrected (lead-dependent systematic MJO error estimated and removed) anomaly correlations are also shown for the forecasts initialized when the MJO was active (labeled "active corrected"). Also shown in (a) is the anomaly correlation for the canonical MJO (i.e., a simple empirical model), which is formed by lag regression of the verifying analyses onto the leading two PCs of OLR at the initial forecast time.

the relevant/recent "mean" state (e.g., 45-day average conditions prior to forecast) and the low-frequency modes of interest (in this case, obtained via time filtering). Krishnamurti *et al.* (1990) argue that this will delay the "contamination of the low-frequency modes as a result of the energy exchanges from the higher frequency modes."

The above idea was tested using a T21 version of the Florida State University (FSU) global spectral model (Krishnamurti *et al.*, 1990). Observed SSTAs, filtered to include only 30–50-day variability (Krishnamurti *et al.*, 1988) and multiplied by a factor of 3.5 to help account for the coarse vertical/boundary-layer structure (i.e., 8 total layers), were specified in addition to the mean annual cycle of SST. While the

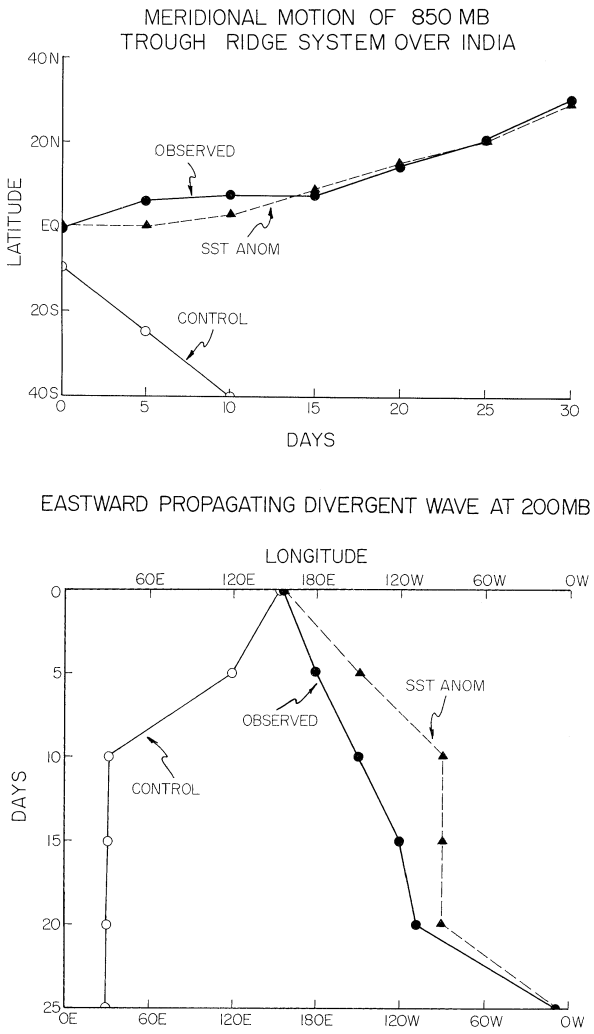

Figure 12.11. (*top*) A y–t diagram of the monsoonal low-frequency ridge line at 850 hPa. The results are shown for the observations, control experiment (no SSTA and complete initialized state), and the SSTA experiment (SSTA specified and initialized state includes time-mean and low-frequency mode only. (*bottom*) Same as (*top*), except an x–t diagram of the position of the 200-hPa divergent center. See text for details of experimental set-up and dates of forecasts. From Krishnamurti *et al.* (1990).

latter specification certainly provides the hindcast with information that a true forecast would not have, the results from the 270-day forecast case study performed from 31 July, 1979, were still encouraging given that intraseasonal SSTAs are not a dominant control at this timescale (Chapters 7, 10, and 11). Figure 12.11 shows that the model forecast exhibited considerable skill at predicting

the meridional motion of the 850-hPa trough–ridge system over India and the eastward propagation of the 200-hPa divergence anomaly out to about 4 weeks. A control experiment that included all frequencies and wave numbers associated with the initial conditions (that the model would accommodate) and that did not include the SSTAs actually performed quite poorly in the first few days. In addition, it was found that if only the mean annual cycle of SST is specified, the amplitude of the low-frequency wave motion degrades considerably, thus indicating the importance of such SSTAs in such an experiment. In Krishnamurti *et al.* (1992, 1995), analogous experiments using two select case studies were performed for low-frequency "wet and dry spells" over China and Australia for each of their associated summer monsoons with essentially the same results as those indicated. As in the first study, the SSTAs were found to be vital to retaining the forecast skill. In both of these studies, simple empirical prediction of the SSTAs was incorporated and found to provide much of the necessary SST information to retain most of the long-lead forecast skill found in this suite of experiments.

12.4 PREDICTABILITY

The previous two sections provide some indication of what the inherent predictability limit might be for the MJO. From the empirical model studies, this limit might be ascertained to be at least 20–30 days. However, as with any empirical model, these models are limited in the totality of the weather/climate system they can predict, their ability to adapt to arbitrary conditions, and their ability to take advantage of known physical constraints. Thus one might conclude that if dynamical models had a realistic representation of the MJO, this limit might be extended somewhat. However, the information that can be ascertained from the above mentioned dynamical studies regarding the intrinsic predictability of the MJO is limited, due to the fact that they were either based on models with a relatively poor representation of the MJO (e.g., weak amplitude and relative fast phase propagation) or they were based on only a few select cases. Moreover, since all the dynamical studies discussed above were verified against observations, their degradation in skill with lead time includes the component associated with the natural limit of predictability of the MJO phenomenon as well as a model's systematic bias associated with the MJO.

A complimentary avenue of research for ascertaining the inherent limits of prediction for the MJO could be derived from so-called "twin-predictability" experiments in which the model employed is presumed to be "perfect" and forecast experiments are verified against others that only differ in the initial conditions (e.g., Lorenz, 1965; Shukla, 1985). This approach was taken in two recent studies by Waliser *et al.* (2003b, c). The important consideration for a study such as this is that the model provides a relatively realistic representation of the phenomenon of interest. In this case, the experiments were performed with the NASA Goddard Laboratory for Atmosphere's (GLA) GCM (Kalnay *et al.*, 1983; Sud and Walker, 1992). In a number of studies, this model has been shown to exhibit a relatively

realistic MJO (Slingo *et al.*, 1996; Sperber *et al.*, 1997; Waliser *et al.*, 2003d) with reasonable amplitude, propagation speed, surface flux properties, seasonal modulation, and interannual variability (IAV) (Waliser *et al.*, 2001). One of its principal deficiencies is its relatively weak variability in the equatorial Indian Ocean, a problem quite common in AGCMs (Waliser *et al.*, 2003d).

For these studies, a 10-year control simulation using specified annual cycle SSTs was performed in order to provide initial conditions from which to perform an ensemble of twin-predictability experiments. Note that this analysis was performed separately on northern hemisphere winter MJO activity (i.e., that which typically travels eastward along the equator and South Pacific Convergence Zone (SPCZ); e.g., Figure 4.5) and northern hemisphere summer MJO activity (i.e., that which typically travels north-eastward into Indian/South East Asia; e.g., Figure 4.10). The following discussion describes the northern hemisphere winter study (Waliser *et al.*, 2003b) but the methods and results are quite similar for the northern hemisphere summer analog (Waliser *et al.*, 2003c). Initial conditions were taken from periods of strong MJO activity identified via extended EOF analysis of 30–90-day band-passed tropical rainfall during the Oct–Apr season. From the above analysis, 15 cases were chosen when the MJO convection was located over the Indian Ocean, maritime continent, western Pacific Ocean, and central Pacific Ocean, respectively, making 60 cases in total. In addition, 15 cases were selected which exhibited very little to no MJO activity. Two different sets of small random perturbations, determined in a rather *ad hoc* and simplistic manner, were added to these 75 initial states. Simulations were then performed for 90 days from each of these 150 perturbed initial conditions.

A measure of potential predictability was constructed based on a ratio of the signal associated with the MJO, in terms of band-passed (30–90-day filter) rainfall or 200-hPa velocity potential (VP200), and the mean square difference between sets of twin (band-passed) forecasts. Predictability was considered useful if this ratio was greater than one, and thus if the mean square error was less than the signal associated with the MJO. The results indicate that useful predictability for this model's MJO extends out to about 20 to 30 days for VP200 and to about 10 to 15 days for rainfall (Figure 12.12). This is in contrast to the timescales of useful predictability for the model's weather, or for cases in which the MJO is absent, which is about 12 days for VP200 and 7 days for rainfall. Note that these latter two regimes are related, in that when the MJO is quiescent, the model lacks a low-frequency component that might help it retain predictability over long timescales and is in a regime where the processes and timescales of weather are the only phenomena left to give predictability. In addition to the above, the predictability measure exhibited modest dependence on the phase of the MJO, with greater predictability for the convective phase at short ($< \sim 5$ days) lead times and for the suppressed phase at longer ($> \sim 15$ days) lead times.

While the results from these studies are encouraging from the view point of subseasonal prediction, and are not entirely inconsistent with the sorts of complimentary studies mentioned above, there are a number of issues to consider that might impact the limit of predictability estimate they provide. First, the model has been

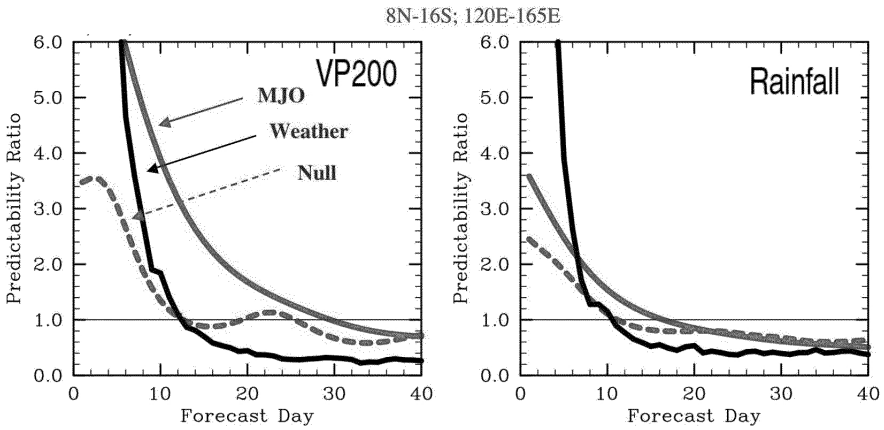

Figure 12.12. Predictability measure (defined as the ratio of the MJO "signal" and the MJO forecast error; see Waliser *et al.*, 2003b) vs. lead time based on 120 northern hemisphere winter MJO twin-predictability forecast cases for VP200 (*left*) and rainfall (*right*) from the NASA GLA model for 120 active/strong MJO cases (solid black), 30 weak/null MJO cases (dashed gray), and the unfiltered "weather" variations (using the 120 active MJO cases; solid gray) for the region 8°N–16°S and 120°E–165°E.

shown to have too much high-frequency low-wave-number activity (Slingo *et al.*, 1996). Relative to the MJO, this variability would be considered to be disorganized, errant convective activity that may erode the relatively smooth evolution of the MJO and thus diminish its predictability. Second, these simulations were carried out with fixed climatological SST values. A previous study with this model showed that coupled SSTs tend to have an enhancing and organizing influence on the MJO, making it stronger and more coherent (Waliser *et al.*, 1999a). Thus the exclusion of SST coupling may lead to an underestimate of the predictability as well. Both of these issues would appear to have a direct relation to the methods and results associated with the Krishnamurti *et al.* studies discussed above.

There are also a number of aspects associated with the model and/or analysis to suggest that the above results might overestimate the predictability of the MJO. The first is that the model's coarse resolution and inherent reduced degrees of freedom relative to the true atmosphere may limit the amount of small-scale variability that would typically erode large time and space scale variability. However, it is important to note in this regard that the low-order EOFs of intraseasonally filtered model output typically do not capture as much variability as analogous EOFs of observed quantities. Thus the model's MJO itself still has room to be more robust and coherent which would tend to enhance predictability. In addition to model shortcomings, the simple manner in which perturbations were added to the initial conditions may also lead to an overestimate of the predictability. The perturbation structure and the size of the perturbations may be too conservative and not adequately represent the type of initial condition error that would be found in an operational context. However, even if that is the case, it would seem that adequate

size "initial" errors would occur in the forecast in a matter of a day or two and thus one would expect this aspect to overestimate the predictability by only a couple of days, if at all.

In order to address some of the uncertainties mentioned above, an analogous study for boreal summer conditions using the European Centre for Medium-range Weather Forecast–Hamburg atmospheric model (ECHAM) AGCM has recently been undertaken (Liess *et al.*, 2004). The modeling and analysis framework is similar to that described above with two important exceptions. First, rather than select a large number of events (i.e., ~15–20) for each of the 4 phases of the boreal summer ISO (i.e., convection in Indian, maritime continent, western Pacific, central Pacific) and performing only a few (i.e., 2) perturbation experiments with each, this study has selected 3 relatively strong events and performs a larger ensemble of forecasts for each of the 4 phases (i.e., 15). In addition, rather than use simply determined perturbations, this study uses the breeding method (Toth and Kalnay, 1993; Cai *et al.*, 2003). The left panels of Figure 12.13 show precipitation (upper) and 200-hPa velocity potential (right) from the individual members of one of the 15-member ensembles (i.e., one phase of one event). Evident is the expected spread of the forecasts with lead time. The right panels of Figure 12.13 quantify this spread in terms of a "signal-to-noise" ratio, defined as in the Waliser *et al.* (2003) study described above. These results suggest that the boreal summer ISO exhibits dynamical predictability with lead times potentially up to and beyond 30 days. These lead times are at least as large, if not larger, than those found in the Waliser *et al.* studies highlighted above. However, it should be noted that the events analyzed here are the strongest 3 events in a 10-year model simulation record, and those above were based on both strong and moderate size events which could account for the difference. In any case, even though the above results do not take into account systematic model bias relative to the observations, they, along with many of the other studies discussed above, indicate that a promising avenue and timescale of operational prediction lies ahead.

12.5 REAL-TIME FORECASTS

Based on the qualified success of some of the MJO prediction efforts discussed above, namely those associated with empirical models, a number of forecast schemes have been implemented in real time. The first of these was associated with the Wheeler and Weickmann (2001) scheme described in Section 12.2. This scheme has been operational for about 3 years and provides forecasts out to about 2–3 weeks lead time for not only the MJO but other coherent modes of tropical variability (e.g., Kelvin waves and mixed Rossby–gravity waves). A second, somewhat related effort, that has been developed more recently builds on the study by Lo and Hendon (2000) and utilizes what is referred to as an all-season Real-time Multivariate MJO (RMM) index (Wheeler and Hendon, 2003). The index results from projecting daily data onto the first two modes of a combined EOF of tropical (15°N–15°S) OLR, and zonal winds at 850 and 200 hPa. This projection

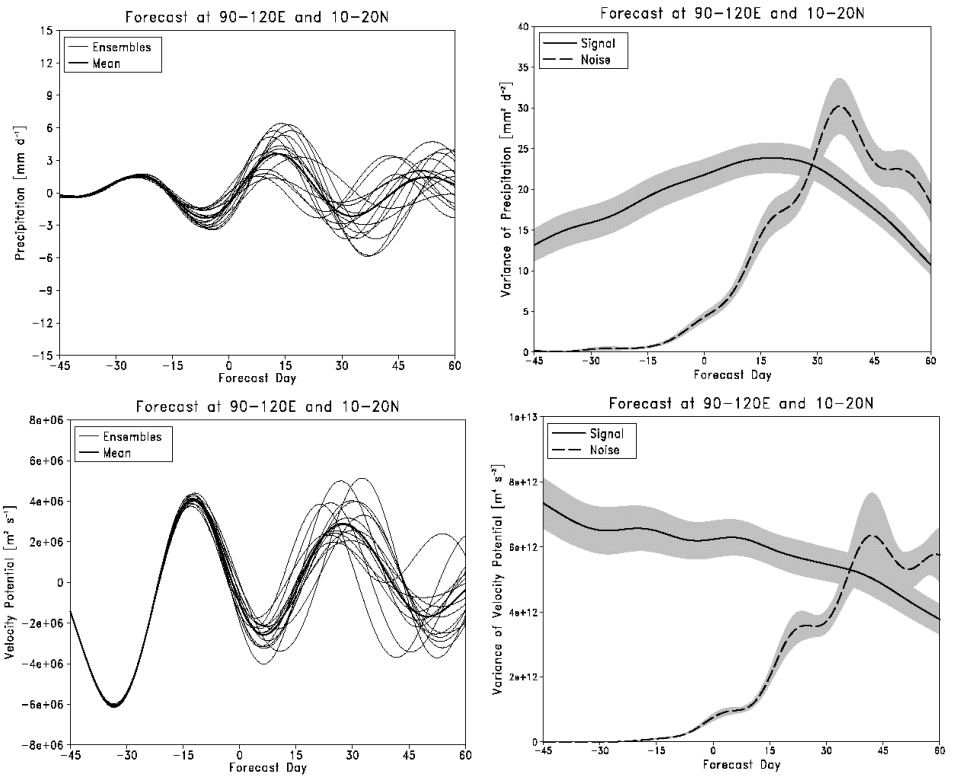

Figure 12.13. (*left*) Fifteen-member ensemble forecast of a boreal summer ISO event, in a given phase of the event (out of four defined phases), using the ECHAM5 AGCM. Data are taken from 90°E–120°E and 10°N–20°N and are 30–90-day filtered precipitation (*upper*) and 200-hPa velocity potential (*lower*) anomalies. (*right*) The signal-to-noise ratios (using the methods in Waliser *et al.*, 2003, see discussion in Section 12.4) for precipitation (*upper*) and 200-hPa velocity potential (*lower*) anomalies when combining 15-member ensembles from 3 different model ISO events and including all 4 phases of each event (i.e., $N = 168$).
From Liess *et al.* (2004).

onto the EOF pair, along with the prior removal of an estimate of the data's very low-frequency components (e.g., ENSO) via their relationship to interannual SST variability, remove the need to perform time filtering to identify the MJO. The values of the index (actually two indices, one amplitude time series for mode 1 (RMM1) and one for mode 2 (RMM2)) at any given time can be used for monitoring. In addition, seasonally and time-lag dependent regression can be used to forecast the evolution of these indices or any associated field, using as predictors RMM1 and RMM2 at the initial day. Skill scores in terms of spatial correlation are about 0.6 for a 12-day forecast and 0.5 for a 15-day forecast. The advantages of the method are that it has a seasonal dependence built in and it can be easily adapted for forecasting nearly any field related to the MJO (see Chapter 5 for more details).

Charles Jones and his colleagues have produced real-time predictions of the MJO for about two years. The scheme utilized has evolved over this time period and the most recent version is described in Jones *et al.* (2003b). The model is based on band-passed (20–90 days) OLR, and zonal winds at 850 and 200 hPa. Upon filtering, a combined EOF of the three fields is computed and then the PCs are separated into summer and winter. A seasonally dependent regression model is then formed at every given lead between 1 and 10 pentads. The model utilizes the first five PCs from the EOF analysis and the five most recent values of the PCs. The model is found to exhibit winter and summer skills comparable to the other empirical models described in Section 12.2.

In quite a different approach, stemming from a somewhat different and/or more comprehensive objective, Matt Newman and his colleagues have developed and implemented a real-time forecasting scheme that has applicability to the MJO based on what is often referred to as the Linear Inverse Model (LIM; Winkler *et al.*, 2001; Newman *et al.*, 2003). The LIM is based on NCEP–NCAR Reanalysis data (Kalnay *et al.*, 1996) that has had the annual cycle removed, been smoothed with a 7-day running mean filter, gridded to T21 spatial resolution, and been reduced by EOF decomposition. The specific fields used include global 250 and 750-hPa streamfunction and tropical column-integrated diabatic heating. For the northern hemisphere winter (summer) model, the first 30 (30) streamfunction and 7 (20) diabatic heating EOFs are used. In this model, historical data are used to define the relationship between a given state (i.e., a weekly average) and conditions one week later, with the process being iterated to produce multi-week forecasts. The advantage of the model is that it includes both tropical (in terms of diabatic heating – hence a prediction of the MJO) and extra-tropical (in terms of streamfunction) forecasts. In this way, the interaction between can be more readily examined and diagnosed. For tropical forecasts of diabatic heating, the LIM slightly outperforms a research version of the NCEP MRF model at lead times of 2 weeks for both northern hemisphere summer and winter, particularly in regions where the MJO is most strongly affecting the diabatic heating field (Figure 12.14).

Van den Dool and Qin (1996) developed a generalized wave propagating forecasting technique that they refer to as "empirical wave propagation" (EWP). EWP is a "phase-shifting" technique that allows one, in the diagnostic step, to determine the amplitude-weighted-average climatological phase speed of anomaly waves (e.g., equatorial MJO), where the waves are represented as either zonal or spherical harmonics. The diagnostic step results in a table of phase speed (or one-day displacement) for waves in the anomaly field as a function of zonal wave number, calendar month, and latitude, based on a specified (model or observed) data set. Its first application was to mid-latitude Rossby waves as diagnosed from 500-hPa geopotential height fields (Qin and van den Dool, 1996). More recently, it has been applied to the MJO (van den Dool and Saha, 2002) and implemented in real time. Figure 12.15 shows the results from the diagnostic step based on analysis of five years of 200-hPa velocity potential analysis data for all seasons. In this case, the wave number 1 disturbance propagates at about $5\,\mathrm{m\,s^{-1}}$ and has an amplitude of about $5 \times 10^6\,\mathrm{m^2\,s^{-1}}$. In the forecast step, given an initial anomaly field, one projects

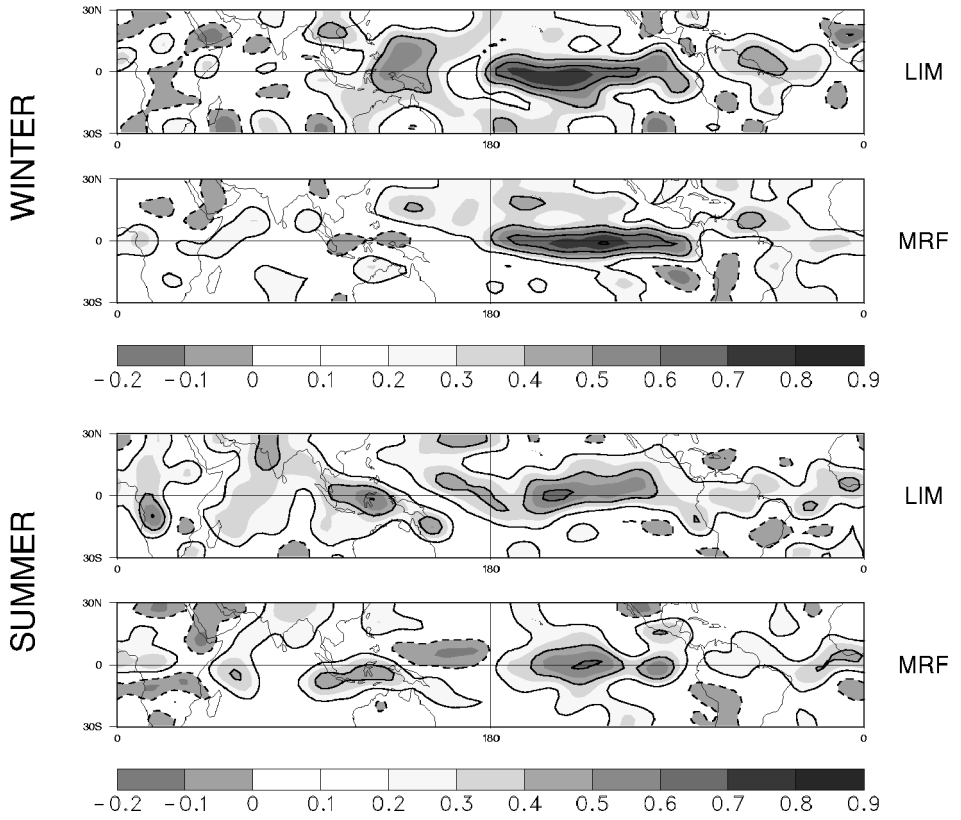

Figure 12.14. Anomaly correlations between forecast and verifiation column-integrated diabatic heating using the LIM forecast model (Winkler *et al*., 2001; Newman *et al*., 2003) and a research version of the NCEP MRF model (i.e., MRF98) for both the northern hemisphere winter (*top*) and summer (*bottom*). Forecasts were made for June–August periods for the years 1979–2000. Solid (dashed) contours indicate positive (negative) values.

the initial condition onto sines and cosines or spherical harmonics, then propagates each wave over the longitude displacement provided by the table, and transforms the field back to physical space. This technique is particularly well suited for empirically forecasting the large-scale upper-level anomalies associated with the MJO.

It is almost a certainty that the MJO's greatest impact based on sheer numbers of people and the severity of losses in agriculture and economics is associated with the Asian summer monsoon. Motivated by this, Webster and Hoyos (2003) have developed an empirical model for predicting Indian district rainfall and the Brahmaputra and Ganges River discharge into Bangladesh on 20–25-day timescales. The empirical model is physically based with predictors drawn from the composite structure of the monsoon ISV (e.g., Indian Ocean SST, precipitation over India, upper level easterly jet, surface winds over the Arabian Sea). In essence, the model

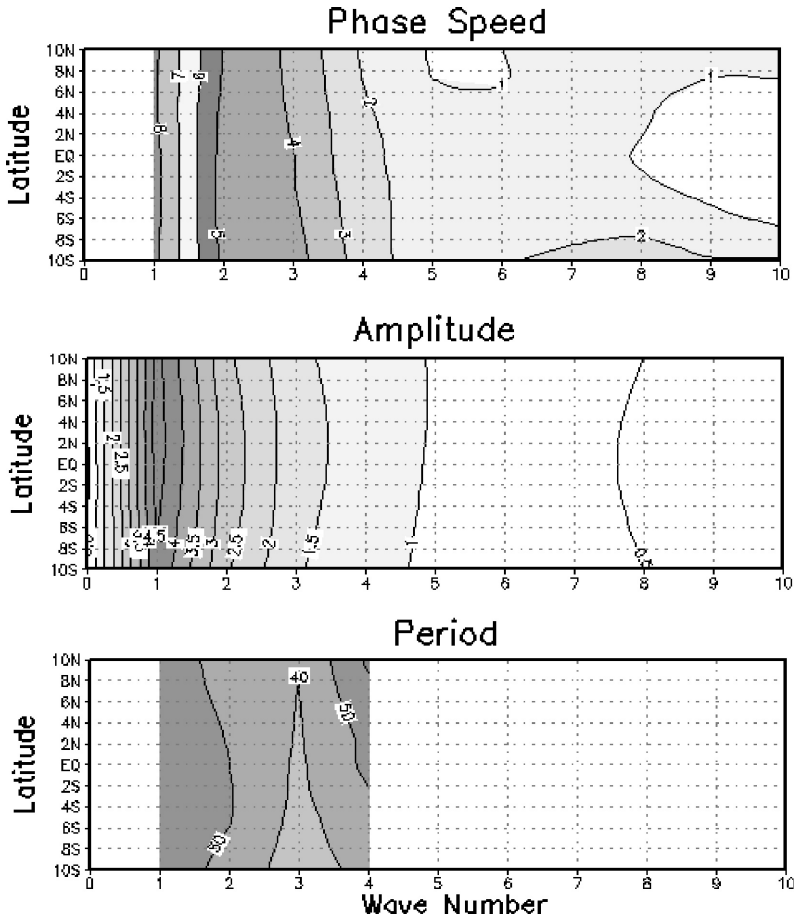

Figure 12.15. Diagnostic information provided by the EWP technique for observed 200-hPa velocity potential anomalies for all seasons combined for the years 1979–1983. The horizontal axis in each plot is global wave number. The units are $\mathrm{m\,s^{-1}}$, $1 \times 10^6\,\mathrm{m^2\,s^{-1}}$, and days, for the upper, middle, and lower plots, respectively.
Based on van den Dool and Qin (1996) and van den Dool (2002).

is Bayesian and uses a wavelet technique to separate significant spectral bands. The model has been used successfully to predict rainfall in hindcast mode. For example, Figure 12.16 shows observed and 20-day forecasts of 5-day average rainfall amounts over the Ganges Valley for the summers of 1999–2002. From these hindcasts, it appears the model is well adept at capturing the seasonal, interannual, and sub-seasonal rainfall variability. The model was also used for the first time during the summer of 2003 in a real-time operational mode in the Climate Forecast Application in Bangladesh project as part of a 3-tier forecasting system wherein seasonal outlooks are given every month for the ensuing 6 months, a 20–25-day forecast is

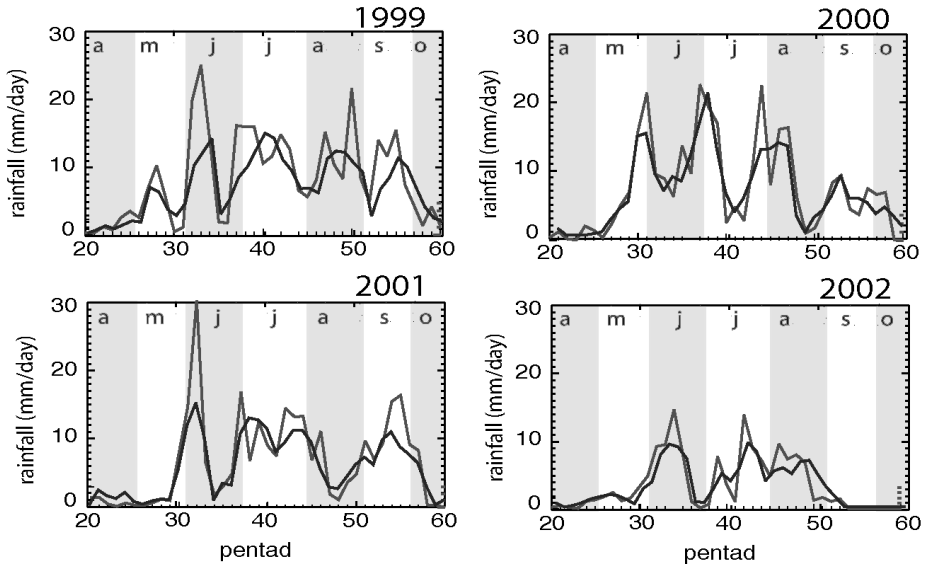

Figure 12.16. Gray lines indicate the forecasts at 20-day (4 pentads) lead time based on the empirical model of Webster and Hoyas (2003) of precipitation averaged over the Ganges Valley for the summers of 1999–2002. Black lines indicate observations. Gray and white background denotes months.

prepared every 5 days, and a 1–5-day forecast is prepared daily. At the time of writing, these forecasts of precipitation and river discharge have been integrated into the Bangladesh forecasting system on an experimental basis.

Based on the sorts of activities and preliminary successes described above, along with the needs to take a more systematic approach to diagnosing problems in dynamical forecasts of the MJO, an experimental MJO prediction program has recently been formulated and is in the process of being implemented. The formal components of this program arose from two parallel streams of activity. The first was the occurrence of the sub-seasonal workshop mentioned in the introduction of this chapter (Schubert *et al.*, 2002) and the recognition of the importance of the MJO in regards to the potential skill to be had from sub-seasonal predictions. The second stream of activity ensued from the priorities and recommendations of the US CLIVAR Asian–Australian Monsoon Working Group (AAMWG). In their 2001 research prospectus (AAMWG *et al.*, 2001) as well as in subsequent deliberations with the US CLIVAR Scientific Steering Committee, recommendations were made to develop an experimental prediction program due to the significant influence that the MJO has on the character and evolution of Asian–Australian monsoons. These streams of activity led to an informal (E-mail) discussion among a number of MJO forecast enthusiasts during the summer and fall of 2002 that helped to formulate the framework for such a program and to the identification of a sponsor that could provide scientific and technical support as well as serve as the data host/server (i.e., NOAA's Climate Diagnostics Center). Invitations to participate in the program were

subsequently sent out to a number of empirical modelers and international forecasting agencies, and an implementation meeting was held in June 2003 (Waliser *et al.*, 2003a).

The motivation for the above experimental program involves not only the obvious objective of forecasting MJO variability but also to serve as a basis for model intercomparison studies. The latter includes using the forecasts and biases in model error growth as a means to learn more about, and possibly rectify, model shortcomings, and also includes using the empirical models to provide some measure of the expectations that should be attributed to the dynamical models in terms of MJO predictive skill. In addition, it is hoped that this program and its forecasts will provide a modeling resource to those trying to diagnose interactions between the MJO and other aspects of weather and sub-seasonal variability (e.g., Pacific–North American (PNA), Arctic Oscillation (AO)). While the immediate goal of the program is to assemble and provide what is readily available from the community in terms of 2–4-week forecasts of the MJO, there are a number of challenges faced by such an effort that are worth highlighting. The most notable involve 1) how to deal with forecast models that have yet or routinely do not have a lead-dependent forecast climatology which is necessary to remove a model's systematic biases, 2) the degree that coupled models and ensembles need to be or can be incorporated into the project, 3) the manner the MJO signal(s) are to be extracted from the heterogeneous set of models (e.g., empirical and numerical), and 4) the general logistical problems of dealing with assembling a very non-uniform set of forecast products from different agencies and researchers in near real time and streamlining them for the purpose of this project.

12.6 DISCUSSION

The review of the studies examined in this chapter was meant to summarize the historical developments associated with MJO forecasting and provide a brief description of the current state of affairs in regards to MJO prediction capability and what is known of its inherent limits of predictability. Overall, there is enough evidence to suggest that MJO prediction can be approached with considerable optimism due to the facts that our capabilities as yet seem far from saturating their potential, and once exploited in an operational sense, will provide a unique and important link between our more mature areas of forecasting, namely weather and ENSO. At present, one of our greatest challenges is still to develop robust and realistic representations of the MJO in our weather and climate forecast models (Chapter 11). Once we have such a capability, we not only have a means to improve predictions of low-frequency weather variations in the tropics that are directly impacted by the MJO, including the onsets and breaks of the Asian and Australian summer monsoons (e.g., Yasunari, 1980; Lau and Chan, 1986; Hendon and Liebmann, 1990a, b; see also Chapters 2, 3, and 5), but we will also likely improve forecasts associated with a number of processes remote to the MJO (see Chapter 4). These include wintertime mid-latitude circulation anomalies (e.g., Weickmann, 1983;

Liebmann and Hartmann, 1984; Weickmann *et al.*, 1985; Lau and Phillips, 1986; Ferranti *et al.*, 1990; Higgins and Schubert, 1996; Higgins and Mo, 1997; Jones *et al.*, 2003a), summertime precipitation variability over Mexico and South America as well as to austral wintertime circulation anomalies over the Pacific–South American sector (e.g., Nogues-Paegle and Mo, 1997; Mo and Higgins, 1998b; Jones and Schemm, 2000; Mo, 2000b; Paegle *et al.*, 2000), extreme events in rainfall variability along the western U.S.A. (e.g., Mo and Higgins, 1998a, c; Higgins *et al.*, 2000; Jones, 2000; Whitaker and Weickmann, 2001), and the development of tropical storms/hurricanes in both the Atlantic and Pacific sectors (Maloney and Hartmann, 2000a, b; Mo, 2000a; Higgins and Shi, 2001).

From the discussion in this chapter, as well as those in Chapters 7, 10, and 11, a number of areas of research and development present themselves. These include a more complete understanding of the role that coupling to the ocean plays in maintaining, and in particular forecasting, the MJO (e.g., Flatau *et al.*, 1997; Wang and Xie, 1998; Waliser *et al.*, 1999a; Kemball-Cook *et al.*, 2002; Fu *et al.*, 2003). For example, a number of recent studies have indicated an error in the phase relation between the convection and SSTAs associated with the MJO in GCM simulations using specified SSTs, whereas coupled simulations tend to reproduce the observed phase relationship (Wu *et al.*, 2002; Fu and Wang, 2003; Zheng *et al.*, 2003). These sorts of studies not only imply the importance of incorporating MJO-related SSTAs but also necessitate they be coupled (i.e., forecast) as well. In addition, there has been virtually no research (albeit the somewhat related work by Krishnamurti *et al.* discussed in Section 12.3) done on model initialization/data assimilation issues in terms of what are the critical criteria to meet in order to adequately initialize the state of the MJO. Related to this are issues regarding the importance of the basic state of the forecast model and how an incorrect basic state might negatively impact the maintenance and propagation of the MJO (Inness *et al.*, 2003; Liess and Bengtsson, 2003; Liess *et al.*, 2003; Sperber *et al.*, 2003). Additional avenues of research include exploring the methods proposed by Krishnamurti *et al.* (1990) with other present-day forecast systems and on more MJO cases as well as exploring the possibility of assimilating empirically-derived forecasts of the MJO into extended-range weather forecasts in order to improve their forecasts of the MJO as well as the remote processes and secondary circulations they interact with. In addition to the above, there is clearly a need for additional dynamical predictability studies of the MJO using other GCMs as well as sensitivity studies to test the effects of SST coupling and ENSO state, the impacts from/on mid-latitude variability, and the influence of the size and type of initial condition perturbations and definition of predictability.

12.7 APPENDIX

Excerpt from John von Neumann (1955):

> It seems quite plausible from general experience that in any mathematical problem it is easiest to determine the solution for shorter periods, over which the extrapolation

parameter is small. The next most difficult problem to solve is that of determining the asymptotic conditions – that is, the conditions that exist over periods for which the extrapolation parameter is very large, say near infinity. Finally, the most difficult is the intermediate range problem, for which the extrapolation parameter is neither very small nor very large. In this case the neglect of either extreme is forbidden. On the basis of these considerations, it follows that there is a perfectly logical approach to any computational treatment of the problem of weather prediction. The approach is to try first short-range forecasts, then long-range forecasts of those properties of the circulation that can perpetuate themselves over arbitrarily long periods of time (other things being equal), and only finally to attempt forecast for medium–long time periods which are too long to treat by simple hydrodynamic theory and too short to treat by the general principles of equilibrium theory.

12.8 ACKNOWLEDGMENTS

This work was supported by the National Science Foundation (ATM-0094416), the National Oceanographic and Atmospheric Administration (NA16GP2021), and the National Atmospheric and Aeronautics Administration (NAG5-11033).

12.9 REFERENCES

AAMWG, US CLIVAR, W. K. M. Lau, S. Hastenrath, B. Kirtman, T. N. Krishnamurti, R. Lukas, J. McCreary, J. Shukla, J. Shuttleworth, D. Waliser, *et al.* (2001) An Asian–Australian Monsoon Research Prospectus by the Asian-Australian Monsoon Working Group, 46 pp.

Barnston, A. G., M. H. Glantz, and Y. X. He (1999) Predictive skill of statistical and dynamical climate models in SST forecasts during the 1997–98 El Niño episode and the 1998 La Niña onset. *Bull. Amer. Meteorol. Soc.*, **80**, 217–243.

Cai, M., E. Kalnay, and Z. Toth (2003) Bred vectors of the Zebiak-Cane model and their potential application to ENSO predictions. *J. Climate*, **16**, 40–56.

Cane, M. A., S. E. Zebiak, and S. C. Dolan (1986) Experimental Forecasts of El-Niño. *Nature*, **321**, 827–832.

Chen, T. C. and J. C. Alpert (1990) Systematic errors in the annual and intraseasonal variations of the planetary-scale divergent circulation in NMC medium-range forecasts. *J. Atmos. Sci.*, **118**, 2607–2623.

Ferranti, L., T. N. Palmer, F. Molteni, and K. Klinker (1990) Tropical–extratropical interaction associated with the 30–60-day oscillation and its impact on medium and extended range prediction. *J. Atmos. Sci.*, **47**, 2177–2199.

Flatau, M., P. J. Flatau, P. Phoebus, and P. P. Niller (1997) The feedback between equatorial convection and local radiative and evaporative processes: The implications for intraseasonal oscillations. *J. Atmos. Sci.*, **54**, 2373–2386.

Fu, X. and B. Wang (2003) Different solutions of intraseasonal oscillation exist in atmosphere–ocean coupled model and atmosphere-only model. *Journal of Climate*, submitted.

Fu, X., B. Wang, T. Li, and J. McCreary (2003) Coupling between northward-propagating boreal summer ISO and Indian Ocean SST: Revealed in an atmosphere–ocean coupled model. *J. Atmos. Sci.*, **60**, 1733–1753.

Goswami, B. N. and P. Xavier (2003) Potential predictability and extended range prediction of Indian summer monsoon breaks. *Geophys. Res. Lett.*, **30**, 1966, doi:10.1029/2003GL017,810.

Graham, N. E. and T. P. Barnett (1995) ENSO and ENSO-related predictability. Part 2: northern-hemisphere 700-Mb height predictions based on a hybrid coupled ENSO model. *J. Climate*, **8**, 544–549.

Hendon, H. H. and B. Liebmann (1990a) The intraseasonal (30–50 Day) oscillation of the Australian summer monsoon. *J. Atmos. Sci.*, **47**, 2909–2923.

Hendon, H. H. and B. Liebmann (1990b) A composite study of onset of the Australian summer monsoon. *J. Atmos. Sci.*, **47**, 2227–2240.

Hendon, H. H., C. D. Zhang, and J. D. Glick (1999) Interannual variation of the Madden–Julian Oscillation during austral summer. *J. Climate*, **12**, 2538–2550.

Hendon, H. H., B. Liebmann, M. Newman, J. D. Glick, and J. K. E. Schemm (2000) Medium-range forecast errors associated with active episodes of the Madden–Julian Oscillation. *Mon. Weather Rev.*, **128**, 69–86.

Higgins, R. W. and S. D. Schubert (1996) Simulations of persistent North Pacific circulation anomalies and interhemispheric teleconnections. *J. Atmos. Sci.*, **53**, 188–207.

Higgins, R. W. and K. C. Mo (1997) Persistent North Pacific circulation anomalies and the tropical intraseasonal oscillation. *J. Climate*, **10**, 223–244.

Higgins, R. W. and W. Shi (2001) Intercomparison of the principal modes of interannual and intraseasonal variability of the North American Monsoon System. *J. Climate*, **14**, 403–417.

Higgins, R. W., J. K. E. Schemm, W. Shi, and A. Leetmaa (2000) Extreme precipitation events in the western United States related to tropical forcing. *J. Climate*, **13**, 793–820.

Inness, P. M., J. M. Slingo, E. Guilyardi, and J. Cole (2003) Simulation of the Madden–Julian Oscillation in a coupled general circulation model. Part II: The role of the basic state. *J. Climate*, **16**, 365–382.

Jones, C. (2000) Occurrence of extreme precipitation events in California and relationships with the Madden–Julian Oscillation. *J. Climate*, **13**, 3576–3587.

Jones, C. and J. K. E. Schemm (2000) The influence of intraseasonal variations on medium- to extended-range weather forecasts over South America. *Mon. Wea. Rev.*, **128**, 486–494.

Jones, C., D. E. Waliser, J. K. E. Schemm, and W. K. M. Lau (2000) Prediction skill of the Madden and Julian Oscillation in dynamical extended range forecasts. *Clim. Dyn.*, **16**, 273–289.

Jones, C., D. E. Waliser, K. M. Lau, and W. Stern (2003a) The Madden–Julian Oscillation and its impact on Northern Hemisphere weather predictability. *Mon. Wea. Rev.*, submitted.

Jones, C., L. M. V. Carvalho, R. W. Higgins, D. E. Waliser, and J. K. E. Schemm (2003b) Statistical forecast skill of tropical intraseasonal convective anomalies. *J. Climate*, submitted.

Kalnay, E., M. Kanamitsu, R. Kistler, W. Collins, D. Deaven, L. Gandin, M. Iredell, S. Saha, G. White, J. Woollen, *et al.* (1996) The NCEP/NCAR 40-year reanalysis project. *Bull. Amer. Meteorol. Soc.*, **77**, 437–471.

Kalnay, E. R., W. Balgovind, D. Chao, J. Edelmann, L. Pfaendtner, I. Takacs, and K. Takano (1983) *Documentation of the GLAS fourth order general circulation model* (Volume 1, NASA Tech. Memo. No. 86064). NASA Goddard Space Flight Center, Greenbelt, M.D.

Kemball-Cook, S., B. Wang, and X. Fu (2002) Simulation of the ISO in the ECHAM4 model: The impact of coupling with an ocean model. *J. Atmos. Sci.*, **59**, 1433–1453.

Keppenne, C. L. and M. Ghil (1992) Adaptive filtering and prediction of the Southern Oscillation index. *J. Geophys. Res. Atmos.*, **97**, 20449–20454.

Kirtman, B. P., J. Shukla, B. H. Huang, Z. X. Zhu, and E. K. Schneider (1997) Multiseasonal predictions with a coupled tropical ocean–global atmosphere system. *Mon. Wea. Rev.*, **125**, 789–808.

Kousky, V. E. and M. T. Kayano (1993) Real-time monitoring of intraseasonal oscillations. 18th Annual Climate Diagnostics Workshop, 1–5 November, 1993, Boulder, CO.

Krishnamurti, T. N., D. K. Oosterhof, and A. V. Mehta (1988) Air sea interaction on the time scale of 30 to 50 days. *J. Atmos. Sci.*, **45**, 1304–1322.

Krishnamurti, T. N., S. O. Han, and V. Misra (1995) Prediction of the dry and wet spell of the Australian monsoon. *Int. J. Climatol.*, **15**, 753–771.

Krishnamurti, T. N., M. Subramaniam, D. K. Oosterhof, and G. Daughenbaugh (1990) Predictability of low-frequency modes. *Meteorol. Atmos. Phys.*, **44**, 63–83.

Krishnamurti, T. N., M. Subramaniam, G. Daughenbaugh, D. Oosterhof, and J. H. Xue (1992) One-month forecasts of wet and dry spells of the monsoon. *Mon. Wea. Rev.*, **120**, 1191–1223.

Lau, K. M. and P. H. Chan (1986) Aspects of the 40–50 day oscillation during the northern summer as inferred from outgoing longwave radiation. *Mon. Wea. Rev.*, **114**, 1354–1367.

Lau, K. M. and T. J. Phillips (1986) Coherent fluctuations of extratropical geopotential height and tropical convection in intraseasonal time scales. *J. Atmos. Sci.*, **43**, 1164–1181.

Lau, K. M. and F. C. Chang (1992) Tropical intraseasonal oscillation and its prediction by the NMC operational model. *J. Climate*, **5**, 1365–1378.

Liebmann, B. and D. L. Hartmann (1984) An observational study of tropical midlatitude interaction on intraseasonal time scales during winter. *J. Atmos. Sci.*, **41**, 3333–3350.

Liess, S. and L. Bengtsson (2003) The intraseasonal oscillation in ECHAM4. Part II: Sensitivity studies. *Clim. Dyn.*, **22**, 671–688.

Liess, S., D. E. Waliser, and S. Schubert (2004a) Predictability studies of the intraseasonal oscillation with the ECHAM5 GCM. *J. Atmos. Sci.*, submitted.

Liess, S., L. Bengtsson, and K. Arpe (2004b) The Intraseasonal Oscillation in ECHAM4. Part I: Coupled to a comprehensive ocean model. *Clim. Dyn.*, **22**, 653–688.

Lo, F. and H. H. Hendon (2000) Empirical extended-range prediction of the Madden–Julian Oscillation. *Mon. Wea. Rev.*, **128**, 2528–2543.

Lorenz, E. N. (1965) A study of the predictability of a 28-variable atmospheric model. *Tellus*, **17**, 321–333.

Lorenz, E. N. (1982) Atmospheric predictability experiments with a large numerical-model. *Tellus*, **34**, 505–513.

Maloney, E. D. and D. L. Hartmann (2000a) Modulation of eastern North Pacific hurricanes by the Madden–Julian Oscillation. *J. Climate*, **13**, 1451–1460.

Maloney, E. D. and D. L. Hartmann (2000b) Modulation of hurricane activity in the Gulf of Mexico by the Madden–Julian Oscillation. *Science*, **287**, 2002–2004.

Matsuno, T. (1966) Quasi-geostrophic motions in the equatorial area. *J. Met. Soc. Jap.*, **44**, 25–43.

Mo, K. C. (2000a) The association between intraseasonal oscillations and tropical storms in the Atlantic basin. *Mon. Wea. Rev.*, **128**, 4097–4107.

Mo, K. C. (2000b) Intraseasonal modulation of summer precipitation over North America. *Mon. Wea. Rev.*, **128**, 1490–1505.

Mo, K. C. (2001) Adaptive filtering and prediction of intraseasonal oscillations. *Mon. Wea. Rev.*, **129**, 802–817.

Mo, K. C. and R. W. Higgins (1998a) Tropical convection and precipitation regimes in the western United States. *J. Climate*, **11**, 2404–2423.

Mo, K. C. and R. W. Higgins (1998b) The Pacific–South American modes and tropical convection during the Southern Hemisphere winter. *Mon. Wea. Rev.*, **126**, 1581–1596.

Mo, K. C. and R. W. Higgins (1998c) Tropical influences on California precipitation. *J. Climate*, **11**, 412–430.

Neuman, J. V. (1955) Some remarks on the problem of forecasting climate fluctuations. *"Dynamics of Climate": The Proceedings of a Conference on the Application of Numerical Integration Techniques to the Problem of the General Circulation*, Pergamon Press, 137.

Newman, M., P. D. Sardeshmukh, C. R. Winkler, and J. S. Whitaker (2003) A study of subseasonal predictability. *Mon. Wea. Rev.*, **131**, 1715–1732.

Nogues-Paegle, J. and K. C. Mo (1997) Alternating wet and dry conditions over South America during summer. *Mon. Wea. Review*, **125**, 279–291.

Paegle, J. N., L. A. Byerle, and K. C. Mo (2000) Intraseasonal modulation of South American summer precipitation. *Mon. Wea. Rev.*, **128**, 837–850.

Palmer, T. N. (1993) Extended-range atmospheric prediction and the Lorenz model. *Bull. Amer. Meteorol. Soc.*, **74**, 49–65.

Qin, J. and H. M. van den Dool (1996) Simple extensions of an NWP model. *Mon. Wea. Rev.*, **124**, 277–287.

Salby, M. L. and H. H. Hendon (1994) Intraseasonal behavior of clouds, temperature, and motion in the tropics. *J. Atmos. Sci.*, **51**, 2207–2224.

Schemm, J. E., H. M. van den Dool, and S. Saha (1996) A multi-year DERF experiment at NCEP. *11th Conference on Numerical Weather Prediction, August 19–13*, Norfolk, Virginia, 47–49.

Schubert, S., R. Dole, H. M. van den Dool, M. Suarez, and D. Waliser (2002) Proceedings from a workshop on "Prospects for improved forecasts of weather and short-term climate variability on subseasonal (2 week to 2 month) time scales", 16–18 April 2002, Mitchellville, MD, NASA/TM 2002-104606, vol. 23, 171 pp.

Shukla, J. (1985) Predictability. *Adv. Geophys.*, **28B**, 87–122.

Slingo, J. M., K. R. Sperber, J. S. Boyle, J. P. Ceron, M. Dix, B. Dugas, W. Ebisuzaki, J. Fyfe, D. Gregory, J. F. Gueremy, *et al.* (1996) Intraseasonal oscillations in 15 atmospheric general circulation models: Results from an AMIP diagnostic subproject. *Clim. Dyn.*, **12**, 325–357.

Sperber, K. R., J. M. Slingo, P. M. Inness, and W. K. M. Lau (1997) On the maintenance and initiation of the intraseasonal oscillation in the NCEP/NCAR reanalysis and in the GLA and UKMO AMIP simulations. *Clim. Dyn.*, **13**, 769–795.

Sperber, K. R., J. M. Slingo, P. M. Inness (2003) The Madden–Julian Oscillation in GCMs in Research Activities in Atmospheric and Oceanic Modelling, Report No. 33, WMO/TD-No. 1161, p. 09-01.

Sud, Y. C. and G. K. Walker (1992) A review of recent research on improvement of physical parameterizations in the GLA GCM. In: D. R. Sikka and S. S. Singh (eds), *Physical Processes in Atmospheric Models*. Wiley Eastern Ltd., pp. 422–479.

Thompson, P. D. (1957) Uncertainty of initial state as a factor in the predictability of large scale atmospheric flow patterns. *Tellus*, **9**, 275–295.

Toth, Z. and E. Kalnay (1993) Ensemble forecasting at NMC: The generation of perturbations. *Bull. Amer. Meteorol. Soc.*, **74**, 2330–2371.

van den Dool, H. M. (1994) Long-range weather forecasts through numerical and empirical-methods. *Dyn. Atmos. Oceans*, **20**, 247–270.

van den Dool, H. M. and J. Qin (1996) An efficient and accurate method of continuous time interpolation of large-scale atmospheric fields. *Mon. Weather Rev.*, **124**, 964–971.

van den Dool, H. M. and S. Saha (2002) Analysis of propagating modes in the tropics in short AMIP runs. *AMIPII workshop. WMO. Toulouse, November 12–15, 2002.*

Vautard, R. and M. Ghil (1989) Singular spectrum analysis in nonlinear dynamics, with applications to paleoclimatic time-series. *Physica D*, **35**, 395–424.

von Neumann, J. (1955) Some remarks on the problem of forecasting climate fluctuations. *Dynamics of Climate. The proceedings of a conference on the application of numerical integration techniques to the problem of the general circulation*, Pergammon Press, 137.

von Storch, H. and J. Xu (1990) Principal oscillation pattern analysis of the 30- to 60-day oscillation in the tropical troposphere. *Clim. Dyn.*, **4**, 175–190.

Waliser, D., Z. Zhang, K. M. Lau, and J. H. Kim (2001) Interannual sea surface temperature variability and the predictability of tropical intraseasonal variability. *J. Atmos. Sci.*, **58**, 2595–2614.

Waliser, D., S. Schubert, A. Kumar, K. Weickmann, and R. Dole (2003a) Proceedings from a workshop on "Modeling, Simulation and Forecasting of Subseasonal Variability", 4–5 June 2003, University of Maryland, College Park, Maryland, NASA/TM 2003-104606, vol. 25, 67 pp.

Waliser, D. E., K. M. Lau, and J. H. Kim (1999a) The influence of coupled sea surface temperatures on the Madden–Julian Oscillation: A model perturbation experiment. *J. Atmos. Sci.*, **56**, 333–358.

Waliser, D. E., C. Jones, J. K. E. Schemm, and N. E. Graham (1999b) A statistical extended-range tropical forecast model based on the slow evolution of the Madden–Julian Oscillation. *J. Climate*, **12**, 1918–1939.

Waliser, D. E., K. M. Lau, W. Stern, and C. Jones (2003b) Potential predictability of the Madden–Julian Oscillation. *Bull. Amer. Meteor. Soc.*, **84**, 33–50.

Waliser, D. E., W. Stern, S. Schubert, and K. M. Lau (2003c) Dynamic predictability of intraseasonal variability associated with the Asian summer monsoon. *Q. J. R. Meteor. Soc.*, **129**, 2897–2925.

Waliser, D. E., K. Jin, I. S. Kang, W. F. Stern, S. D. Schubert, M. L. Wu, K. M. Lau, M. I. Lee, J. Shukla, V. Krishnamurthy *et al.* (2003d) AGCM simulations of intraseasonal variability associated with the Asian summer monsoon. *Clim. Dyn.*, **21**, 423–446.

Wang, B. and X. S. Xie (1998) Coupled modes of the warm pool climate system. Part 1: The role of air–sea interaction in maintaining Madden–Julian Oscillation. *J. Climate*, **11**, 2116–2135.

Webster, P. J. and C. Hoyos (2003) Forecasting monsoon rainfall and river discharge variability on 20–25 day time scales. *Bull. Amer. Meteorol. Soc.*, in press.

Weickmann, K. M. (1983) Intraseasonal circulation and outgoing longwave radiation modes during northern hemisphere winter. *Mon. Wea. Rev.*, **111**, 1838–1858.

Weickmann, K. M., G. R. Lussky, and J. E. Kutzbach (1985) Intraseasonal (30–60 day) fluctuations of outgoing longwave radiation and 250-Mb stream-function during northern winter. *Mon. Wea. Rev.*, **113**, 941–961.

Wheeler, M. and G. N. Kiladis (1999) Convectively coupled equatorial waves: Analysis of clouds and temperature in the wavenumber–frequency domain. *J. Atmos. Sci.*, **56**, 374–399.

Wheeler, M. and K. M. Weickmann (2001) Real-time monitoring and prediction of modes of coherent synoptic to intraseasonal tropical variability. *Mon. Wea. Rev.*, **129**, 2677–2694.

Wheeler, M. and H. Hendon (2003) An all-season real-time multivariate MJO index: Development of an index for monitoring and prediction. *Monthly Weather Review*, submitted.

Whitaker, J. S. and K. M. Weickmann (2001) Subseasonal variations of tropical convection and week-2 prediction of wintertime western north American rainfall. *J. Climate*, **14**, 3279–3288.

Winkler, C. R., M. Newman, and P. D. Sardeshmukh (2001) A linear model of wintertime low-frequency variability. Part I: Formulation and forecast skill. *J. Climate*, **14**, 4474–4494.

Wu, M. L. C., S. Schubert, I. S. Kang, and D. E. Waliser (2002) Forced and free intra-seasonal variability over the South Asian monsoon region simulated by 10 AGCMs. *J. Climate*, **15**, 2862–2880.

Yasunari, T. (1980) A quasi-stationary appearance of the 30–40 day period in the cloudiness fluctuations during the summer monsoon over India. *J. Met. Soc. Jap.*, **59**, 336–354.

Zheng, Y., D. E. Waliser, W. F. Stern, and C. Jones (2003) The role of coupled sea surface temperatures in the simulation of the tropical intraseasonal oscillation. *J. Climate*, **17**, 4109–4134.